Cell Stem Cell

Article

3D post-implantation co-culture of human embryo and endometrium

Graphical abstract

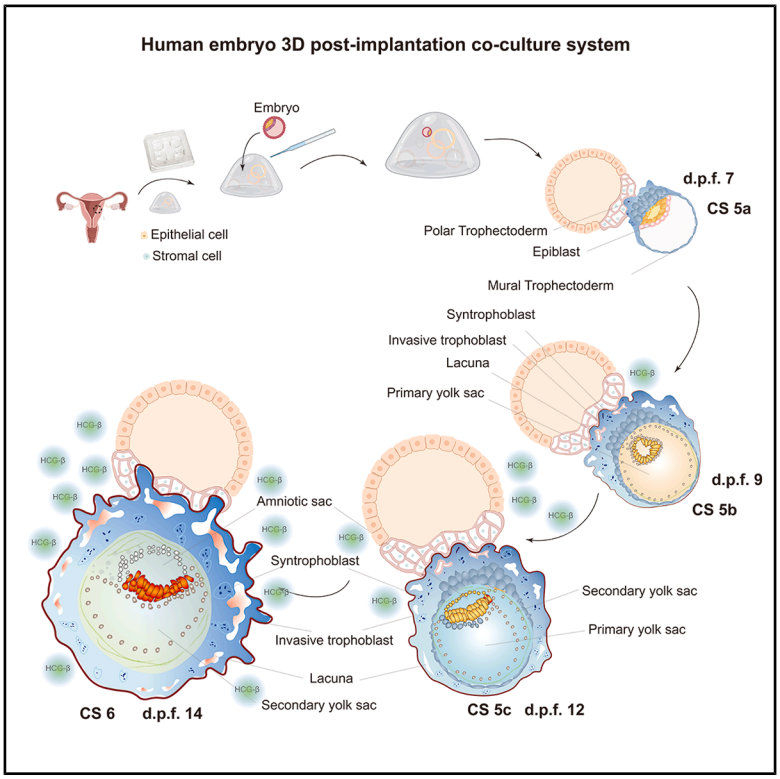

Highlights

- A 3D co-culture system models human embryo-endometrium interactions through d.p.f. 14
- The endometrial niche accelerates extravillous trophoblast emergence
- hCG signaling is essential for embryo adhesion and early development
- Embryo-endometrial co-culture models fetal-maternal crosstalk

Authors

Jinzhu Song, Rusong Zhao, Yu Zhang, ..., Jun Wu, Zi-Jiang Chen, Han Zhao

Correspondence

wukeliang_527@163.com (K.W.), jun2.wu@utsouthwestern.edu (J.W.), chenzijiang@hotmail.com (Z..-J.C.), hanzh80@sdu.edu.cn (H.Z.)

In brief

Zhao and colleagues develop a 3D co-culture system of human embryo and endometrium that mirrors post-implantation development, revealing key signaling events at the maternal-embryonic interface relevant to early pregnancy success.

Song et al., 2026, Cell Stem Cell *33*, 58–72
January 8, 2026
https://doi.org/10.1016/j.stem.2025.12.002

CellPress

CellPress
OPEN ACCESS

Cell Stem Cell

Article

3D post-implantation co-culture of human embryo and endometrium

Jinzhu Song,[1,2,3,13] Rusong Zhao,[1,2,4,5,13] Yu Zhang,[1,2,6,13] Minghui Lu,[1,2] Peishu Liu,[6] Tao Li,[7] Cheng Li,[1,2] Ruijie Yu,[1,2] Xueyao Chen,[1,2] Huajian Yang,[1,2] Xinwen Zhang,[1,2] Yining Su,[1,2] Yanli Han,[1,2] Duanchen Sun,[8] Qingbin Zhou,[8] Zhenzhen Hou,[1,2] Weijing Liu,[1,2] Xiaoyuan Gao,[1,2] Wenrong Tao,[1,2] Jingye Zhang,[1,2] Jingwen Wang,[1,2] Yingying Qin,[1,2,7] Hongmei Wang,[9] Keliang Wu,[1,2,3,*] Jun Wu,[10,11,12,*] Zi-Jiang Chen,[1,2,3,*] and Han Zhao[1,2,3,4,14,*]

[1]State Key Laboratory of Reproductive Medicine and Offspring Health, Center for Reproductive Medicine, Institute of Women, Children and Reproductive Health, Shandong University, Jinan 250012, China
[2]Key Laboratory of Reproductive Endocrinology (Shandong University), Ministry of Education, Jinan 250012, Shandong, China
[3]Research Unit of Gametogenesis and Health of ART-Offspring, Chinese Academy of Medical Sciences (No. 2021RU001), Jinan 250012, Shandong, China
[4]Center for Clinical Reproductive Medicine, the First Affiliated Hospital of Nanjing Medical University, Nanjing 210029, Jiangsu, China
[5]The Affiliated Suzhou Hospital of Nanjing Medical University, Suzhou Municipal Hospital, Gusu School, Nanjing Medical University, Suzhou 215000, Jiangsu, China
[6]Department of Obstetrics and Gynecology, Qilu Hospital of Shandong University, Jinan 250012, Shandong, China
[7]Department of Obstetrics and Gynecology, Shandong Provincial Hospital, Shandong First Medical University, Jinan 250022, Shandong, China
[8]School of Mathematics, Shandong University, Jinan 250100, China
[9]Key State Laboratory of Organ Regeneration and Reconstruction, Institute of Zoology, Chinese Academy of Sciences, Beijing 100101, China
[10]Department of Molecular Biology, University of Texas Southwestern Medical Center, Dallas, TX, USA
[11]Hamon Center for Regenerative Science and Medicine, University of Texas Southwestern Medical Center, Dallas, TX, USA
[12]Cecil H. and Ida Green Center for Reproductive Biology Sciences, University of Texas Southwestern Medical Center, Dallas, TX, USA
[13]These authors contributed equally
[14]Lead contact
*Correspondence: wukeliang_527@163.com (K.W.), jun2.wu@utsouthwestern.edu (J.W.), chenzijiang@hotmail.com (Z.-J.C.), hanzh80@sdu.edu.cn (H.Z.)
https://doi.org/10.1016/j.stem.2025.12.002

SUMMARY

Embryo-maternal interaction is essential for post-implantation human development. While endometrial organoids have enabled *in vitro* modeling of the uterine environment, a fully integrated 3D co-culture system with human embryos has not been established. Here, we develop a physiologically relevant 3D platform that supports the co-culture of human embryos with endometrial organoids, enabling reciprocal embryo-maternal communication. This system sustains development to day 14 post-fertilization with structural and molecular fidelity to Carnegie stage landmarks, including yolk sac formation, primordial germ cell specification, and trophoblast maturation. Single-cell transcriptomics and functional assays reveal that the endometrial niche accelerates extravillous trophoblast emergence at day 9 post-fertilization and primes their invasive programs. Disruption of maternal signals, including human chorionic gonadotropin signaling blockade, markedly impairs embryonic progression. This co-culture system provides a powerful and tractable model to dissect human peri- and post-implantation development, with broad relevance to early pregnancy loss, placental biology, and reproductive medicine.

INTRODUCTION

Successful post-implantation development depends on both a competent blastocyst and a receptive endometrium.[1] The endometrium not only supports blastocyst attachment but also initiates the formation of the maternal-fetal interface, which is essential for continued embryogenesis.[2] Disruptions in trophedctoderm (TE)-endometrium interactions can lead to implantation failure, pregnancy loss, and other complications.[3] Recent studies have extended the culture of human blastocysts beyond implantation stages in the absence of maternal tissues, shedding light on early post-implantation development.[4–7] Parallel efforts have used human pluripotent stem cells to generate 3D embryo-like structures[8–13] that model peri-implantation to early organogenesis stages, providing key insights into human embryogenesis. However, these systems lack maternal components, limiting their ability to fully recapitulate early pregnancy.

To address this, recent studies have explored 2D co-culture systems combining human embryos with endometrial cells to model peri-implantation crosstalk.[14,15] While these efforts have

offered valuable information, they fall short of replicating the complex three-dimensional architecture of the *in vivo* uterine environment. At present, no 3D system exists that faithfully models embryo-maternal interactions during early post-implantation in humans.

Endometrial organoids (EOs)[16,17] have emerged as promising platforms for reconstructing the maternal uterine environment, successfully capturing multiple epithelial and stromal cell types of the endometrium *in vitro*. Building on this, we developed a 3D EO-based platform[16] that mimics the receptive endometrium. In this study, we establish a 3D co-culture system combining human embryos with receptive EOs. This integrated model enables direct embryo-maternal interactions and provides a physiologically relevant system for investigating human post-implantation development.

RESULTS

A 3D co-culture system supports human embryogenesis to d.p.f. 14 with physiological fidelity

To establish a 3D co-culture system recapitulating embryo-endometrial interactions, we combined day 5 post-fertilization (d.p.f.) human blastocysts derived from *in vitro* fertilization (IVF) with receptive EOs that include both epithelial and stromal compartments[16] (Figure 1A). To support the co-culture, we optimized the culture media used for 3D human embryo cultures- (mIVC medium)[4] originally used for extended embryo culture, generating a modified medium compatible with both embryos and EOs (HIVC1 and HIVC2) (see STAR Methods). Blastocysts were initially cultured in HIVC1 medium under 6% CO_2, followed by a switch to HIVC2 medium at 72 h. Half-media changes were performed every other day to maintain nutrient balance and signaling gradients. Both embryos and EOs were maintained in 3D under conditions adapted from protocols used for post-implantation human embryo culture[4] (see STAR Methods), enabling extended co-development within a physiologically relevant microenvironment.

To assess developmental progression in our 3D co-culture model, we performed daily bright-field imaging and time-lapse video microscopy from d.p.f. 5 to 14 and compared the results with Carnegie stage (CS) human embryos[18–21] at equivalent stages (Figures 1B and S1A; Video S1). Embryos displayed continued growth and dynamic morphogenesis throughout this period. Within 12 h of co-culture initiation, TE cells began migrating toward and establishing connections with the EOs, initiating stable intercellular connections. By d.p.f. 6, embryos had attached to the EOs (Video S1). At d.p.f. 7, the polar trophectoderm penetrated the EO and began proliferating actively, whereas the mural trophectoderm remained as a monolayer of flattened cells. The epiblast (EPI) exhibited its first proliferative expansion, displaying histoarchitectural features consistent with CS5a *in vivo*. By d.p.f. 9, the trophectoderm had expanded into a multilayered structure, forming a clearly visible chorionic cavity (CHC) and establishing a deeply interdigitated interface with the underlying endometrial tissue. At the same time, the nascent primary yolk sac (PYS) emerged *de novo*, recapitulating key *in vivo* developmental landmarks. Notably, these features have not been reported in previous embryo culture systems lacking maternal tissue support[4–6] (Figures 1B and S1A). From d.p.f. 9 to 14, the EPI continued to proliferate, and the yolk sac (YS) lumen enlarged, paralleling *in vivo* developmental progression. The entire conceptus underwent substantial volumetric expansion and further penetration into the EOs. Time-lapse imaging revealed that this invasive advance proceeded through alternating cycles of compaction and expansion—rather than continuous linear growth—suggesting a previously unrecognized mode of tissue-level remodeling. In accordance with ethical guidelines, all experiments were terminated at d.p.f. 14.

To assess the impact of endometrial co-culture on embryonic development, we compared co-cultured embryos with embryo-only controls using bright-field imaging. From d.p.f. 9 to 12, control embryos displayed reduced translucency under the stereo microscopy, indicating impaired formation and expansion of embryonic cavities (Figures 1B and S1A; Video S1). Additionally, surface trophectoderm cells in controls began to loosen and slough off, suggesting the onset of apoptosis in superficial TEs. Quantitative analysis revealed a significantly higher survival rate in co-cultured embryos: 75% (15/20) survived to d.p.f. 14, compared with 37.5% (6/16) in the control group (Figures S1A and S1B). Co-cultured embryos were also markedly larger—averaging 399.7 ± 31.6 μm in diameter at d.p.f. 9 versus 332.4 ± 71.2 μm in controls, and 695.8 ± 64.3 μm at d.p.f. 14 versus 465.4 ± 129.5 μm in controls (Figure S1C). These morphometric values more closely align with reference Carnegie collection embryo measurements.[18–21] All co-cultured embryos successfully adhered to EOs, with ∼81% (13/16) showing polar attachment (Figures S1D–S1F). Collectively, these findings demonstrate that human embryos maintained in a 3D embryo-endometrium co-culture system exhibit substantially enhanced viability, growth, and developmental progression compared with those cultured alone.[4–6] The spatiotemporal progression of key morphogenetic processes—including EPI proliferation, cavity formation, and TE invasion—faithfully recapitulates *in vivo* development, both structurally and quantitatively, according to Carnegie standards.[18–21]

To further characterize developmental progression, we performed transmission electron microscopy (TEM) on a d.p.f. 9 embryo displaying disc-like morphology consistent with CS5. Toluidine blue-stained 2-μm semi-thin sections revealed clear structural features of post-implantation development, including the pro-amnion (AME) cavity, YS, extraembryonic mesoderm (EXM), CHC, and distinct maternal-fetal contact zones between TEs and the EO (Figure 1C). These findings closely mirror those observed in Carnegie specimen no. 8171,[18,19] underscoring the physiological fidelity of the co-culture system. We also performed scanning electron microscopy (SEM) on a fractured d.p.f. 12 embryo to examine surface and internal architecture. The internal view exposed a well-defined embryonic disc composed of columnar EPI cells (length: 172.9 μm, width: 68.6 μm), morphologically comparable to Carnegie specimen no. 7700.[20] The external surface exhibited numerous protruding TE villi, indicating active interactions with the maternal-like environment (Figure 1D).

Co-culture enables trilineage specification and timely EVT emergence

To rigorously assess embryonic development in the co-culture system, morphologically normal embryos were subjected to

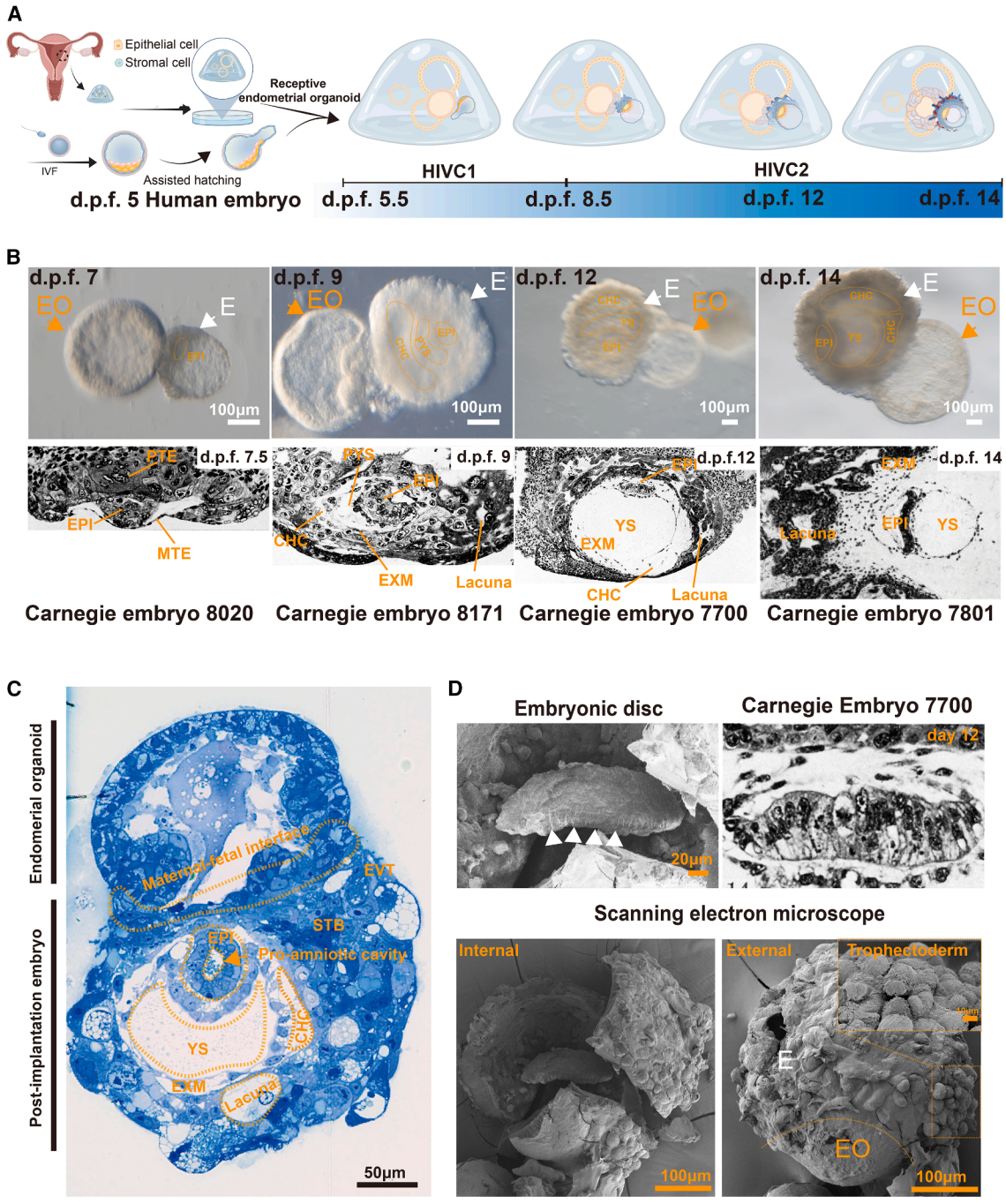

Figure 1. Human embryos organize with endometrial tissues in the 3D post-implantation co-culture system

(A) Schematic illustration of a 3D *in vitro* post-implantation co-culture platform for human embryo and endometrium.

(B) Bright-field images of human embryos organized with endometrial tissues at different time points. White arrowheads denote embryo. Yellow arrowheads denote endometrial organoid (EO). The bottom row, from left to right, corresponds to the developmental stages under a light microscope, with CS images reproduced from *in vivo* human embryonic development[18–21] and schemes of early post-implantation human embryos at CS5a (day 7.5), CS5b (day 9), CS5c (day 12), and CS6a (day 14). EPI, epiblast; PTE, polar trophoblast; MTE, mural trophoblast; EXM, extraembryonic mesoderm; PYS, primary yolk sac; YS, yolk sac; CHC, chorionic cavity.

(C) Semi-thin sectioning images for TEM Sample Localization with toluidine blue staining of a co-cultured human embryo and EO. Yellow arrowheads denote pro-amniotic cavity.; EVT, extravillous trophoblast.

(D) SEM images of a d.p.f. 12 embryo. It showed the internal and external structure of the embryo and magnified the morphological structure of the embryonic disc (the CS5c embryonic disc, 0.204 × 0.165 mm on the right)[20] and trophectoderm. White arrowheads denote columnar cells in the embryonic disc.

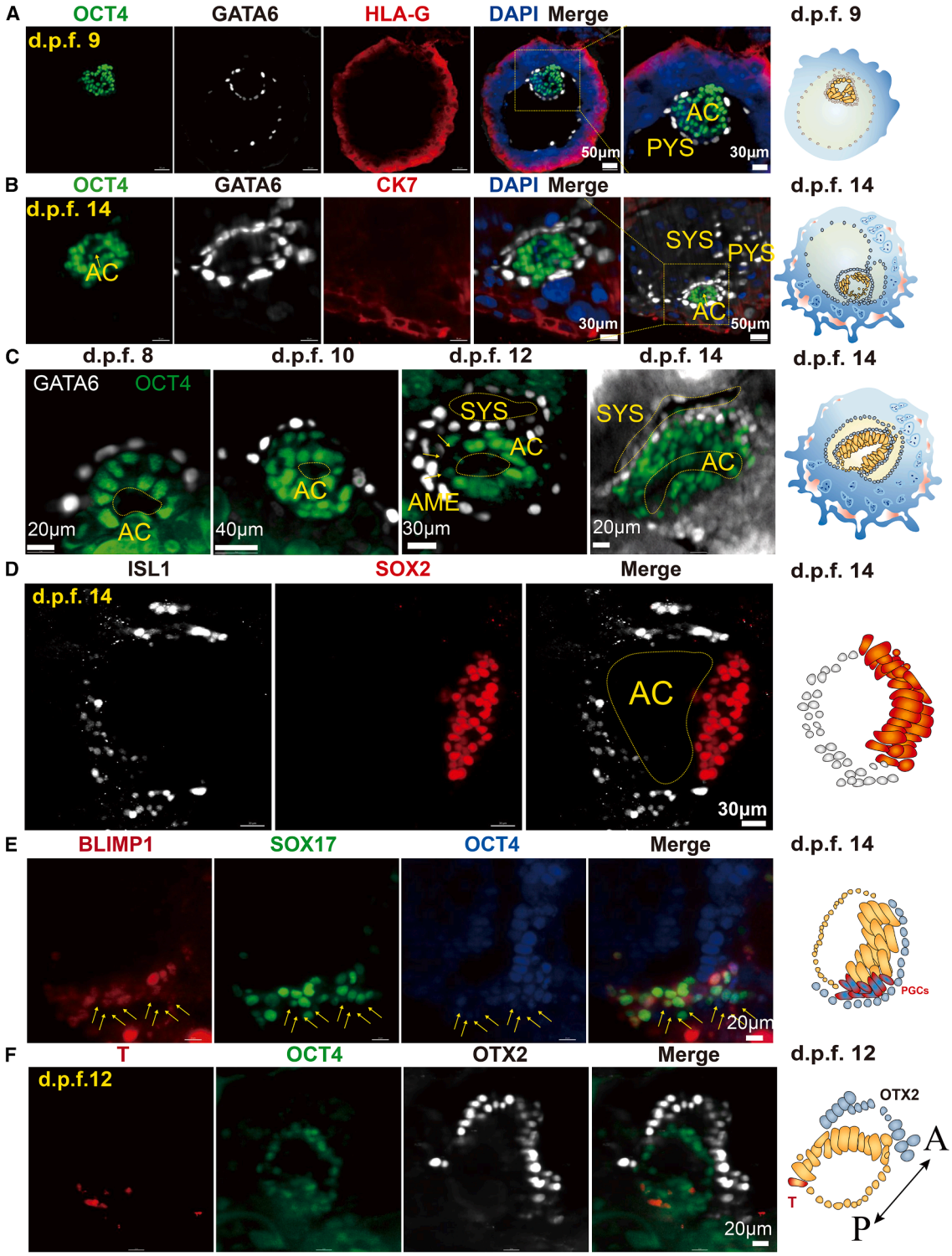

Figure 2. The post-implantation embryos in the co-culture system undergo lineage morphogenesis and EMT

(A) Representative immunofluorescence (IF) images of embryos at d.p.f. 9 (7 out of 7 embryos) and fixed for whole-mount staining with antibodies for OCT4 (green), HLA-G (red), and GATA6 (white). Scale bar, 50 μm. Magnification of inner cell mass (yellow dotted lines). Scale bar, 30 μm.

(B) Representative IF images of embryos at d.p.f. 14 (3 out of 3 embryos) and fixed for whole-mount staining with antibodies for OCT4 (green), CK7 (red), and GATA6 (white). Scale bar, 50 μm. Magnification of inner cell mass (yellow dotted lines). Scale bar, 30 μm.

(legend continued on next page)

whole-mount clearing followed by lineage-specific immunostaining. We examined specification across three embryonic compartments—EPI, hypoblast (HYPO), and TE—using OCT4 (EPI), GATA6 (HYPO), CK7 (TE), and HLA-G (extravillous trophoblast [EVT]) markers (Figures 2A and 2B). By d.p.f. 9, OCT4$^+$ EPI cells began organizing around a pro-amniotic cavity, while GATA6$^+$ HYPO and HLA-G$^+$ TE cells occupied distinct spatial domains. Notably, co-cultured embryos generated HLA-G$^+$ EVT cells, as confirmed by time-lapse imaging and histology, which indicated active invasion into the EO (Figure 2A). This milestone mirrors the timing of EVT emergence *in vivo*.[18] At d.p.f. 14, OCT4$^+$ EPI cells expanded, GATA6$^+$ HYPO cells outlined a defined YS cavity, and CK7$^+$ TE cells encased the outer layer with abundant cytoplasm. While the morphology and size of the EPI diverged from those seen in CS6 embryos, the secondary YS (SYS) formed in a manner largely consistent with natural development, prompting further investigation of EPI status (Figure 2B). From d.p.f. 8 to 14, we tracked morphological transitions in OCT4$^+$ and GATA6$^+$ cell populations across serial time points. These analyses revealed the coordinated emergence of both the SYS and AME, demonstrating that the EO co-culture platform supports key lineage decisions and spatial organization events (Figure 2C).

To stage d.p.f. 14 embryos and assess developmental competence within the co-culture system, we examined the embryonic-disc architecture via immunostaining for ISL1 and SOX2 (Figure 2D). In line with previous findings,[10] ISL1 was robustly expressed in a population of squamous dorsal cells, while SOX2 expression was notably reduced—features indicative of AME identity (Figure 2D). Three-dimensional reconstruction of the fluorescent signals revealed that the SOX2$^+$ EPI-like region formed a distinct discoidal structure surrounding an enlarged AME-like cavity (Figure S2A). This spatial arrangement closely mirrors the architecture observed in CS6a embryos from the Carnegie collection.[21]

To determine whether primordial germ cell (PGC) specification occurs in d.p.f. 14 co-cultured embryos, we applied a validated triple-marker immunostaining panel—OCT4, SOX17, and BLIMP1—that defines bona fide human PGCs[22] (Figure 2E). This analysis revealed discrete clusters of PGC-like cells located immediately beneath the EPI, recapitulating the anatomical positioning and molecular signature of *in vivo* PGC emergence. These findings provide evidence that the co-culture system faithfully recapitulates the temporal and spatial dynamics of early human germline specification.

To map the developmental trajectory of human embryos within the co-culture system, we combined SEM morphometry with whole-mount immunofluorescence analysis of d.p.f. 12 conceptuses. This multimodal approach delineated the onset of amniogenesis and the establishment of embryonic polarity. Immunofluorescence revealed presumptive EPI cells with diminished OCT4 expression—an early hallmark of amniotic lineage commitment—coinciding with low-level Vimentin immunoreactivity,[23] indicative of incipient epithelial-to-mesenchymal transition (EMT) and the initiation of amniogenesis (Figure S2B). Simultaneously, spatially distinct immunolocalization patterns of OTX2/T and CER1/T in d.p.f. 12 embryos demonstrated mutual exclusion, confirming proper anterior-posterior (A-P) axis specification (Figures 2F and S2C). By d.p.f. 14, the embryonic-disc displayed well-polarized primitive streak formation, verified by the spatially restricted domains of T and OCT4/SOX17 expression (Figure S2D). EMT-associated morphological changes aligned closely with those of Carnegie specimen no. 7950,[24] providing *in vivo* morphological validation (Figure S2E). Together, these structural and molecular analyses confirm that the embryos in co-culture undergo coordinated lineage specification and morphogenesis with high fidelity to the *in vivo* spatiotemporal developmental program.

TE subtypes recapitulate *in vivo* maturation and function

To validate light and electron microscopy findings indicating TE differentiation consistent with *in vivo* development (Figures 1B and 1C), we performed comprehensive immunofluorescence profiling at d.p.f. 9 and 14 (Figure 3).

At d.p.f. 9, immunolabeling with DAPI, phalloidin, human chorionic gonadotropin (HCG)-β, and luteinizing hormone/choriogonadotropin receptor (LHCGR) revealed abundant HCG-β$^+$ syncytiotrophoblasts (STBs) concentrated on the TE surface. Notably, HCG-β$^+$ STBs were also found infiltrating both apical and basal zones of the EO (Figures 3A and 3B). Lacunae-like cavities emerged within the proliferating cytotrophoblast (CTB) core, mirroring features in toluidine blue-stained sections and highly reminiscent of Carnegie embryo no. 8171.[18,19] This architectural arrangement confirms the presence of both primitive invasive STBs,[25] which disrupt epithelial junctions to facilitate endometrial invasion, and post-invasive STBs,[25] which remodel endometrial glands into nutrient-filled lacunae (Figures 3A and 3B). In parallel, HLA-G$^+$ spindle-shaped EVTs[26]—a hallmark of deeper invasion—were observed actively penetrating the EO, mimicking the morphology of EVTs seen in Carnegie embryo no. 8004 (Figure 3C). These features have not been previously documented *in vitro* at such an early developmental stage.

By d.p.f. 14, triple-lineage immunostaining revealed a complete repertoire of TE identities: GATA3$^+$/TEAD4$^+$ CTBs, SDC-1$^+$/HCG-β$^+$ STBs,[27] and HLA-G$^+$ EVTs (Figures 3D–3F). The toluidine blue image shows lacunae that appear to lie adjacent to the endometrium (Figure 3D). Immunofluorescence staining of stage-matched embryos reveals that these lacunae remain enclosed by STB. Importantly, comparable lacunar structures are also observed within TE populations that are not in direct contact with the endometrium, indicating that their formation is not restricted to regions

(C) Human blastocysts were cultured until d.p.f. 8, 10, 12, and 14 and fixed for whole-mount staining with antibodies for OCT4 (green, EPI marker) and GATA6 (white, HYPO marker). Yellow dotted lines: AC and SYS. Scale bar, 20 μm, 40 μm, 30 μm, and 20 μm.

(D) Human blastocysts were cultured until d.p.f. 14 (3 out of 3 embryos) and fixed for whole-mount staining with antibodies for ISL1 (white, amniotic marker) and SOX2 (red, EPI marker). Scale bar, 30 μm. Yellow dotted lines: AC.

(E) Lightsheet Z-sections of d.p.f. 14 embryos, showing progenitor germ cells (PGCs) with co-expression of BLIMP1 (red), SOX17 (green), and OCT4 (blue). Scale bar, 20 μm. Yellow arrows denote BLIMP1$^+$, SOX17$^+$, and OCT4$^+$ cells.

(F) As shown by the yellow snip, the location of T-expressing EPI was opposite to the anterior visceral endoderm (OTX2) side (2 out of 2 embryos). Scale bar, 20 μm.

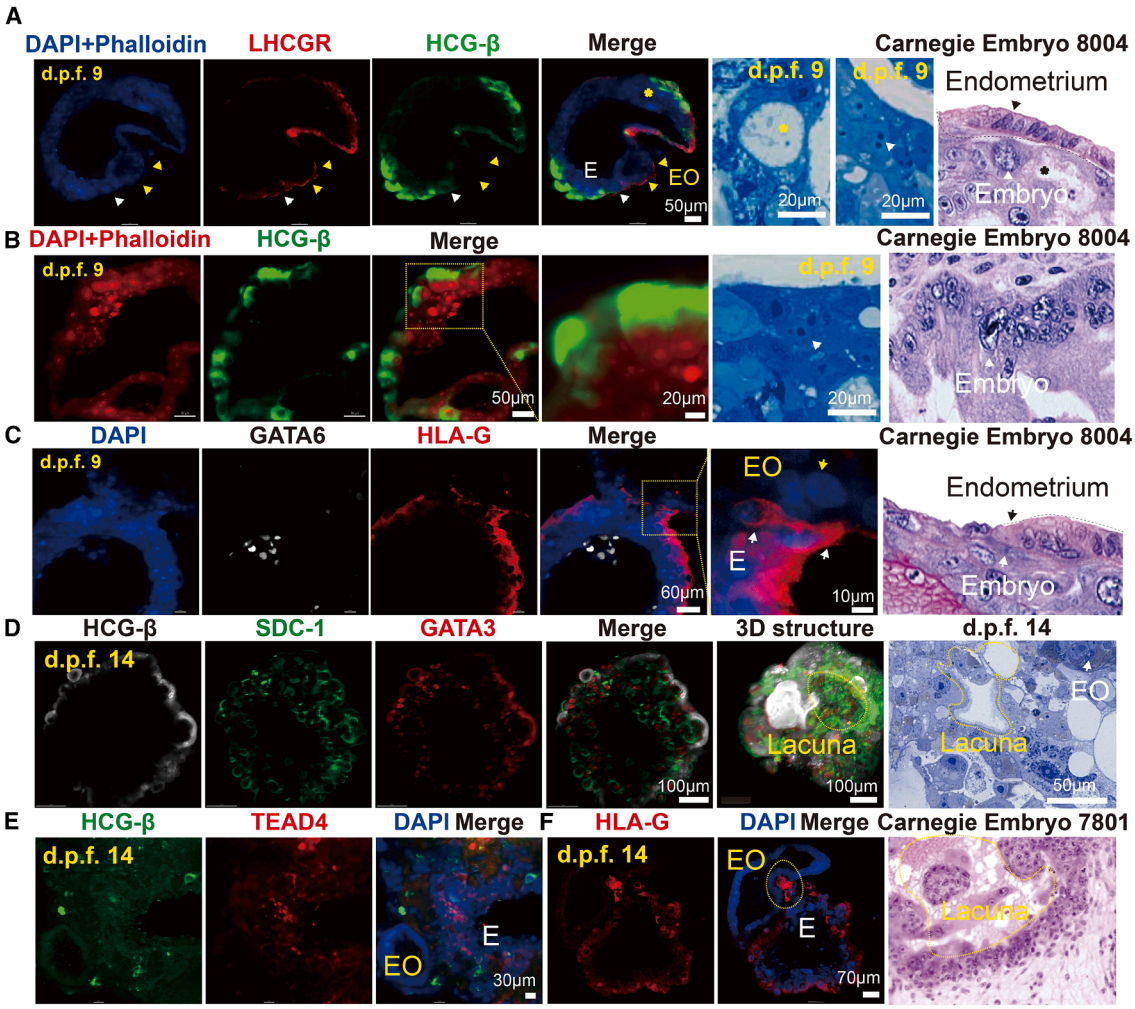

Figure 3. The post-implantation embryos in the co-culture system differentiate into functional TEs earlier than pure cultured embryos

(A) Human blastocysts were cultured until d.p.f. 9 (3 out of 3 embryos) and fixed for whole-mount staining with antibodies for DAPI and phalloidin (blue), HCG-β (green, syncytiotrophoblast [STB] marker), and LHCGR (red). Scale bar, 50 μm. Yellow arrows: endometrial organoids (EOs); white arrows: embryo (E); yellow asterisks: lacuna. Right: serial toluidine blue TEM sections of a d.p.f. 9 co-culture embryo. Scale bar, 20 μm. Yellow asterisk, lacuna; white arrowheads, STB cells in direct contact with EO cells. Magnified view of the maternal-embryonic interface in Carnegie embryo no. 8004[18,19], at the equivalent developmental stage. White arrowheads, STB at the contact surface; black arrows, uterine luminal epithelial cells; black asterisk, lacuna.

(B) Human blastocysts were cultured until d.p.f. 9 (3 out of 3 embryos) and fixed for whole-mount staining with antibodies for DAPI and phalloidin (red) and HCG-β (green, STBs marker). Scale bar, 50 μm and 20 μm. Yellow dotted lines: STBs. Right: sequential toluidine blue TEM sections of a d.p.f. 9 co-culture embryo (left) and a magnified view of the implantation site in Carnegie embryo no. 8004[18,19] at the equivalent stage (right). White arrowheads indicate STB cells located at the trophoblast (TE) surface that correspond to IF signals; in both samples these STB cells are situated at the deepest point of embryonic invasion into the uterine tissue.

(C) Representative IF images of embryos at d.p.f. 9 (3 out of 3 embryos) fixed for whole-mount staining with antibodies for DAPI (blue), GATA6 (white), and HLA-G (red). Scale bar, 60 μm and 20 μm (magnification). Yellow arrows: EOs; white arrows: embryo (E). Right, magnified view of the maternal-embryo interface in Carnegie embryo no. 8004[18] equivalent stage. White arrowheads indicate elongated, spindle-shaped HLA-G$^+$ extravillous trophoblast (EVT) cells at the contact surface; black arrows denote uterine luminal epithelial cells.

(D) Lightsheet Z-sections of d.p.f. 14 embryos marked co-immunostaining of the multiple TE marker genes with HCG-β (white), SDC1 (green), and GATA3 (red) (2 out of 2 embryos). Scale bar, 100 μm. Highlighted structures illustrate the formation of lacuna. Right: toluidine blue TEM section of a d.p.f. 14 co-culture embryo. Scale bar, 50 μm. The yellow dashed line demarcates the mature lacunar structure corresponding to that observed in IF. A white arrowhead: the endometrial-organoid (EO) domain.

(E) Lightsheet Z-sections of d.p.f. 14 embryos marked co-immunostaining of the multiple TE marker genes with HCG-β (green) and TEAD4 (red, CTB marker) (2 out of 2 embryos). Scale bar, 30 μm. EOs, endometrial organoids.

(F) Lightsheet Z-sections of d.p.f. 14 embryos marked co-immunostaining of the multiple TE marker genes with HLA-G (red) (2 out of 2 embryos). Scale bar, 70 μm. Yellow highlighted structures denote extravillous trophoblasts (EVTs). EOs, endometrial organoids. Right: magnified view of a mature lacunar structure within the TE of Carnegie embryo no. 7801[21] at the corresponding stage. Yellow dashed line outlines the lacuna. The toluidine blue-stained sections shown in (D) were prepared from different embryos of the same developmental stage and batch as those used for IF staining. These embryos were cultured *in vitro* under identical conditions.

immediately apposed to the maternal tissue. EVTs were enriched at the embryo-maternal interface and represented a significantly greater fraction of the TE population than at d.p.f. 9, indicating continued TE maturation (Figure 3F).

During early pregnancy, the uterine endometrium transforms into decidua, critical for implantation and pregnancy maintenance. Receptive EOs exhibited robust expression of hormone-responsive implantation markers, including ERα, PRA/B, and FOXO1 (Figures S3A–3C; Video S2). EOs contained luminal epithelial cells (WNT7A$^+$), glandular epithelium (FOXA2$^+$), immune cells (CD45$^+$), and stromal fibroblasts (Vimentin$^+$) (Figures S3D–3G; Video S3). Co-culture with embryos from d.p.f. 11 to 14 induced marked upregulation of FOXO1,[28] HAND2,[29] and DKK1[30]—key regulators of decidual markers (Figure S4A). Additionally, we observed decreased KI67 and increased caspase-3 (CC3) expression, indicating reduced proliferation and increased apoptosis,[31] hallmarks of physiological decidual transformation (Figure S4B). These results suggest that embryo-derived cues trigger the *in situ* decidual program of EOs, further reinforcing the physiological relevance of the co-culture system.

Single-cell transcriptomics reveals endometrial-induced EVT acceleration

To dissect embryonic lineage dynamics and maternal influences at single-cell resolution, we performed single-cell RNA sequencing (scRNA-seq) on co-cultured embryos at d.p.f. 9 (n = 25), 12 (n = 16), and 14 (n = 33) (Figures 4A and 4B; Video S4). Souporcell[32]-based genetic demultiplexing distinguished maternal from fetal cells using SNP profiles (Figure 4C). Uniform manifold approximation and projection (UMAP) clustering resolved major embryonic lineages—EPI, HYPO, and EXM—alongside diverse maternal EO populations (Figure 4D; Table S1). The proportion of EXM cells rose to 13.76% of all embryonic cells by d.p.f. 14. Transcriptional identities corresponded to canonical lineage markers (Figure S5A; Table S2). Integrated analysis with reference datasets revealed close alignment of co-cultured embryos to *in vivo* CS7[33] gastrulation-stage profiles (Figures 4E, 4F, and S5B), and EO transcriptional signatures matched receptive-phase endometrium (Figures S5C and S5D). Kyoto encyclopedia of genes and genomes (KEGG) pathway analysis showed EXM cells enriched for ECM and cytoskeleton-related genes (e.g., *COL1A1*, *THBS1*, and *CD44*), and EOs enriched for interleukin (IL)-17 signaling, mineral absorption, and placental development pathways (Figure S5A; Table S2). These findings confirm that the co-culture system faithfully models transcriptional features of post-implantation human development.

Pseudotime trajectory mapping revealed temporally synchronized differentiation of EPI and HYPO, with EXM specification peaking by d.p.f. 14 (Figures S5E and S5F). EXM cells progressively upregulated cytoskeletal and ECM-interaction genes (*COL3A1*, *COL5A1*, and *VIM*) (Figures S5A and S4F; Table S2). EOs concurrently activated gene modules associated with placental signaling and maternal-fetal communication (Figure S5A). Focused subclustering of the TE compartment identified clear CTB, STB, and EVT populations (Figures 4G, 4H, and S6A), each with distinct stage-specific expression dynamics. STBs showed enrichment in syncytialization-related pathways, including ER stress response and Golgi transport, suggestive of functional hormone and protein trafficking roles (Figure S6B). Trajectory analysis revealed a branching lineage path, with CTBs giving rise to both STBs and EVTs. This differentiation was accompanied by temporal activation of transcription factors and effector genes, such as *GATA3*, *TFAP2A*, *CCR7*, *KRT7*, and *HCG* (Figures 4I, 4J, S6C, and S6D; Table S3). These data highlight a tightly regulated gene network guiding TE lineage bifurcation, maturation, and functional specialization.

Accelerated EVT maturation and invasion induced by endometrial co-culture

To directly assess the influence of the endometrial niche on TE development—and to independently validate the early appearance of EVTs at d.p.f. 9 (Figures 2A and 3C), a phenomenon not observed in embryo-only culture systems—we integrated our scRNA-seq data from co-cultured embryos with published datasets of embryos cultured without EOs at d.p.f. 10–14 (Figures 5A, 5B, and S7A). Despite globally conserved TE differentiation trajectories and clustering patterns across datasets (Figures 5A, 5B, and S7B), co-culture significantly altered gene expression across CTB, EVT, and STB populations (Figure S7C; Table S4). Notably, co-culture upregulated genes involved in adherens junction formation and ECM-receptor signaling (e.g., *CTNNB1*, *PARD3*, *EGFR*, *ITGA2/6*, and *LAMA1/C1*), while downregulating a subset of canonical TE markers (*CGA*, *CGB3*, and *HLA-G*) and ribosomal genes (Figure S7C). Crucially, these transcriptomic changes corroborated immunofluorescence-based detection of HLA-G$^+$ EVTs at d.p.f. 9 (Figures 2A, 3C, and 5C), indicating that endometrial co-culture not only promoted the early emergence of EVTs—3 days earlier than in standard culture—but also induced a ∼2-fold increase in EVT abundance by d.p.f. 12–14 (Figure 5C). Pseudotime trajectory analysis confirmed an accelerated EVT maturation profile in co-cultured embryos (Figure S7B), and functional enrichment analyses highlighted activation of key pathways related to extracellular matrix remodeling, estradiol responsiveness, and placental development (Figure 5D). Transcriptomic consistency was independently validated using switching mechanism at 5′ end of the RNAtranscript2 (Smart-seq2) (Figure S7D), and comparative analyses across datasets revealed co-culture-specific deviations from both conventional *in vitro* and *in vivo* benchmarks (Figures S7E and S7F). Together, these findings provide robust molecular evidence that the endometrial environment instructs and accelerates EVT lineage specification and maturation.

Human EVTs, derived from the blastocyst trophectoderm, differentiate into two principal subtypes: interstitial (iEVTs) and endovascular (eEVTs).[34] scRNA-seq profiling of co-cultured and solo-cultured embryos revealed a conserved hierarchy of EVT differentiation, progressing from proliferative EVT1 precursors to transitional EVT2 states and ultimately to invasive iEVTs. eEVTs were not detected in either condition prior to d.p.f. 14 (Figures 5E–5G and S7H). Notably, endometrial co-culture markedly accelerated this developmental cascade, triggering iEVT emergence as early as d.p.f. 9—3 days earlier than observed in solo-cultured embryos—and significantly expanding the EVT1 compartment (Figures 5F and 5G). Pseudotime analysis confirmed temporal compression of the EVT1 → EVT2 → iEVT transition within the d.p.f. 9–14 window (Figure S7J), aligning with key developmental

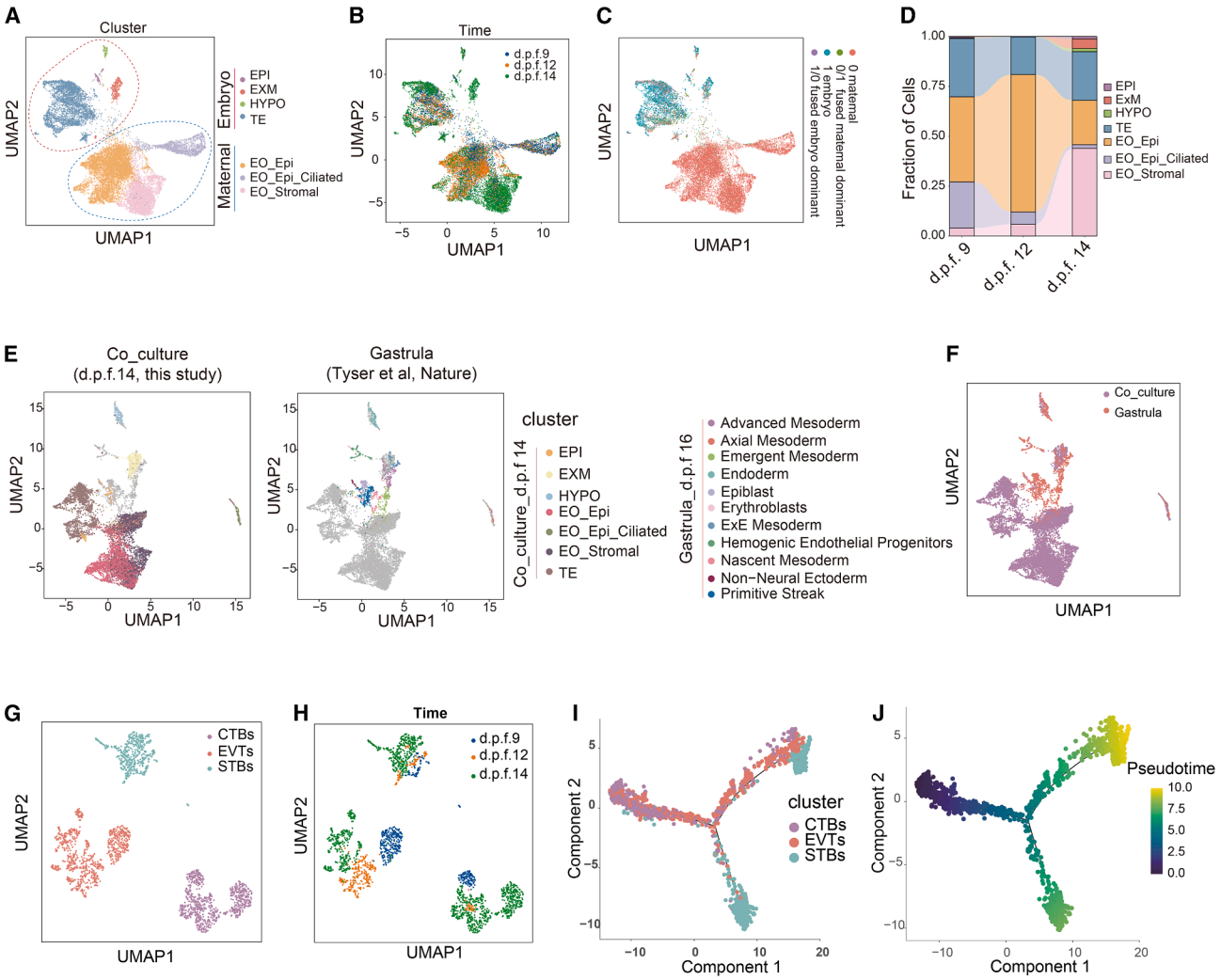

Figure 4. Single-cell transcriptomics reveals distinct embryonic and maternal cell populations during co-culture development

(A and B) UMAP analyses revealing seven clusters, identified as the EPI (epiblast), EXM (extraembryonic mesoderm), HYPO (hypoblast), TE (trophoblast), EO_Epi (unciliated epithelium of organoid), EO_Epi_Ciliated (ciliated epithelium of organoid), and EO_Stromal (stromal cell of organoid) based on classical lineage-specific marker expression (A) and development time (d.p.f. 9, $n = 25$; d.p.f. 12, $n = 16$; and d.p.f. 14, $n = 33$) (B).

(C) UMAP plot showing the cellular source of early human embryo-maternal development identified by the souporcell package. "0" indicates maternal cells. "1" indicates embryo cells. "0/1" and "1/0" indicate fused maternal or embryo cells dominant, respectively.

(D) The percentage of each cell type in relation to the total sequenced population for each sample.

(E and F) UMAP analyses revealing the comparison between our co-cultured system (d.p.f. 14) and a CS7 gastrulation-stage embryo, highlighting the cellular source (F) and cell types (E).

(G and H) UMAP analyses revealing three clusters, identified as the STBs (syncytiotrophoblast), EVTs (extravillous trophoblast), and CTBs (cytotrophoblasts) based on classical lineage-specific marker expression (G) and development time (d.p.f. 9, 12, and 14) (H).

(I and J) Single-cell pseudotime trajectory indicating the differentiation of CTB, EVT, and STB clusters in our co-cultured embryos.

milestones. Co-cultured iEVTs exhibited transcriptional hallmarks of functional maturation, including elevated expression of lineage-defining regulators (*PLAC8* and *SERPINE2*) (Figure S7I) and pro-invasive effectors such as *IL6*, *CXCL1/2*, *ITGA2*, *MMP9*, and *ITGB6*. These cells also showed robust enrichment of IL-17 and tumor necrosis factor (TNF) signaling pathways implicated in placental giant cell differentiation and spiral artery remodeling[34] (Figure 5H). Together, these data demonstrate that the endometrial microenvironment acts not merely as a permissive scaffold but as an instructive niche that functionally primes iEVTs for placental bed invasion through accelerated lineage commitment and activation of key invasion programs.

Ultrastructural and molecular characterization of the embryo-endometrial interface

To elucidate the structural basis of early maternal-fetal communication, we acquired high-resolution confocal images and generated detailed three-dimensional reconstructions, capturing key embryonic cavity features and spatial arrangements at the embryo-endometrial interface (Figure S8A; Video S5).

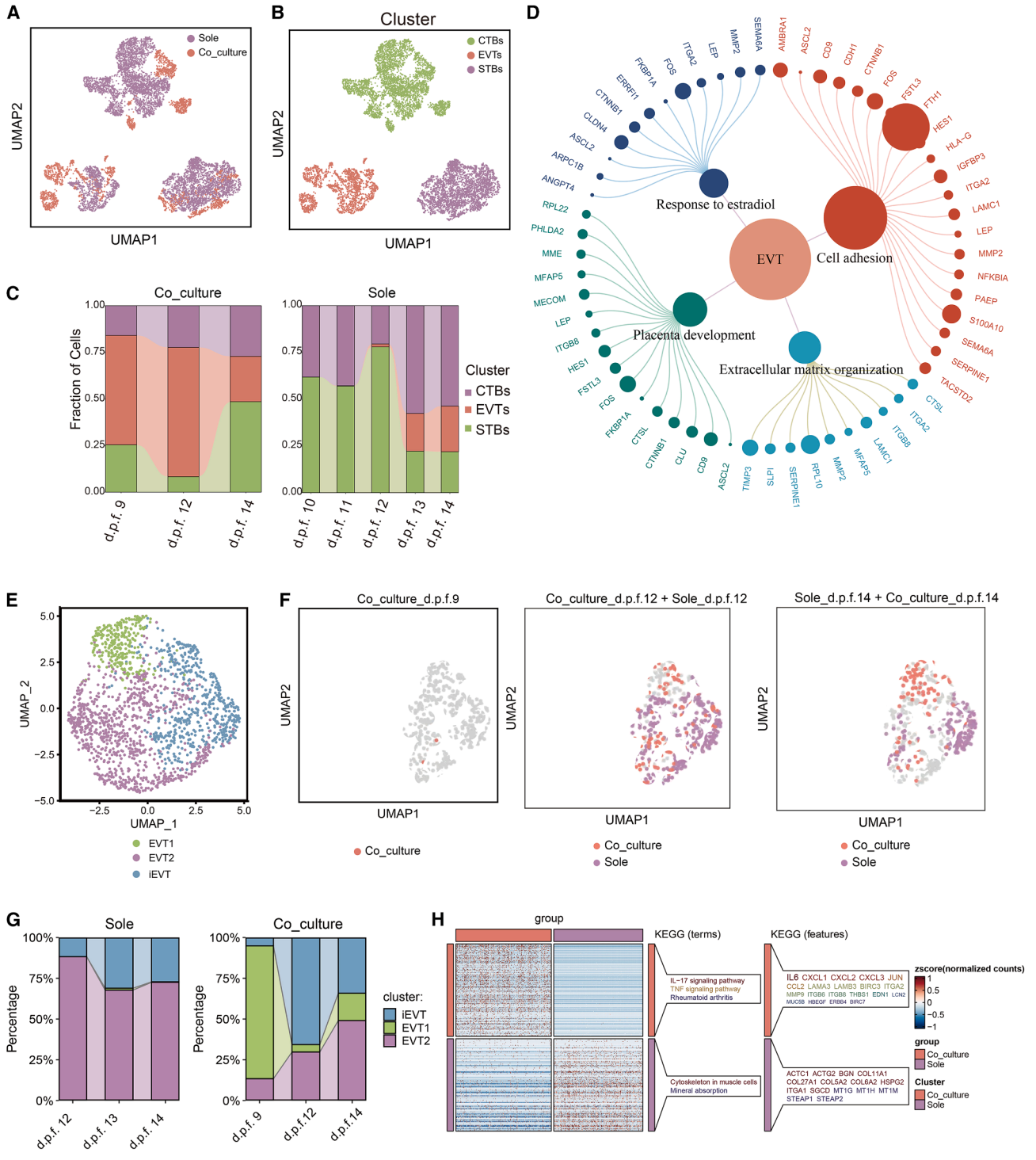

Figure 5. Endometrial co-culture accelerates extravillous TE emergence

(A and B) UMAP analysis from TEs of sole embryos and co-cultured embryos, identified as the CTB (cytotrophoblast), EVTs (extravillous trophoblasts), and STB (syncytiotrophoblast).

(C) The percentage of each cell type in relation to the total sequenced population for each sample.

(D) Network diagram showing the representative GO functions of EVT and the corresponding key genes and pathways.

(E) UMAP plots illustrating the comparison of iEVT, EVT1, and EVT2 of sole embryos and co-cultured embryos.

(legend continued on next page)

Complementing this, we conducted SEM and TEM to define ultrastructural signatures of early attachment (Figure 6A). SEM revealed striking morphological contrasts: the EO surface exhibited irregular bulging topography, in contrast to the smoother trophectodermal surface, suggesting spatially distinct adhesion domains. TEM identified lipid- and protein-rich vesicular structures[35] on trophectoderm cells (Figure 6B), which progressively accumulated along microvillous projections (Figure 6C) and were accompanied by a loosening of intercellular junctions.[36–38] These vesicles clustered along nascent villous protrusions[38] (Figure 6C), consistent with localized secretion and signaling functions. On the maternal side, the glandular epithelium displayed prominent pinopodes[39] and dense electron-dense globules (Figure 6D), hallmark features of a decidualizing endometrium. Together, these ultrastructural findings illuminate the interplay between post-implantation embryonic TE and endometrial cells, underscoring a dynamic, spatially resolved vesicle-mediated signaling niche at the embryo-maternal interface.

To resolve the cellular architecture and molecular mediators within the implantation niche, we performed immunofluorescence staining for lineage-specific markers. Formation of fused, multinucleated syncytia was evident, with hCG signals prominently outlining enlarged nuclear domains, consistent with active syncytialization (Figure S8B; Video S6). Co-staining for SOX17—a marker of endometrial glandular epithelium—and the TE marker GATA3 delineated opposing cellular architectures at the interface, visualizing juxtaposed maternal and fetal compartments (Figure S8C). The transcription receptor NR2F2, expressed in both TE and endometrial lineages, further highlighted cell-type-specific morphologies: enlarged, irregular syncytial nuclei in the TE compartment versus uniform, compact nuclei in the endometrial epithelium (Figure S8D). Notably, HLA-G$^+$ signals emerged at d.p.f. 9, marking discrete invasion foci and forming structural projections reminiscent of *in vivo* maternal-fetal anchoring bridges (Figure 3C). Together, these results identify hCG and HLA-G as key molecular effectors of TE syncytialization and embryo-endometrium integration.

To dissect the molecular logic governing intercompartmental communication during implantation, we integrated spatial proteomics (SP) and single-cell ligand-receptor interaction analyses. SP of the d.p.f. 9 embryo-EO interface revealed localized enrichment of laminin-integrin signaling modules (Figures 6E, S8E, and S8F), implicating these adhesive and matrix-stabilizing pathways as key mediators of embryo-uterine anchorage.[40–44] To further resolve intercellular communication dynamics, we re-analyzed our scRNA-seq dataset using CellPhoneDB v.4,[45] quantifying ligand-receptor pairings over time. This analysis revealed progressive amplification of juxtacrine signaling between TE subtypes (EVTs and STBs) and maternal epithelial and stromal cells, with a marked increase in interaction complexity from d.p.f. 9 to 14 (Figures 6F and S8G). Notably, leukemia inhibitory factor-leukemia inhibitory factor receptor (LIF-LIFR) and colony stimulating factor 1-colony stimulating factor 1 receptor (CSF1-CSF1R) signaling, initially localized to the EO, became progressively enriched in the trophectoderm as development advanced (Figures 6G and S8G). By contrast, TE-derived cues such as interleukin 6-interleukin 6 receptor (IL-6-IL-6R), cytochrome P450 family 19 subfamily A member 1-estrogen receptor 1 (CYP19A1-ESR1), and leptin-leptin receptor (LEP-LEPR) shifted toward the EO, establishing reciprocal communication circuits (Figures 6G and S8G). This reciprocal ligand-receptor signaling network establishes a dynamic molecular dialogue that drives coordinated maturation of the trophectoderm-endometrium interface.

Functional validation identifies hCG-LHCGR signaling as a critical regulator of embryo adhesion

To functionally interrogate a key pathway implicated in embryo-endometrial communication, we disrupted hCG-LHCGR signaling. Immunofluorescence analysis revealed perinuclear localization of LHCGR colocalized with β-hCG in STBs (Figure 6H), consistent with autocrine/paracrine activation. Neutralization of hCG using a blocking antibody profoundly impaired embryo-EO attachment and developmental progression (Figure 6I). At d.p.f. 6, ∼50% of control embryos adhered to EOs, whereas none of the hCG-blocked embryos exhibited attachment. By d.p.f. 10, maternal-fetal contact was observed in 87.5% of controls but only 37.5% of treated embryos, and no embryos in the hCG-inhibited group progressed beyond the d.p.f. 9 morphological stage (Figure 6J). These findings establish embryonic hCG as a master regulator of implantation competence, essential for both adhesive integration and post-adhesion development. In addition to reinforcing its status as a clinically validated biomarker of pregnancy viability, our data provide mechanistic insight into how impaired hCG signaling may underlie early pregnancy failure.

Together, these functional and molecular analyses delineate a coordinated signaling program wherein endometrial cues direct initial adhesion via laminin-integrin scaffolding, while reciprocal embryonic signals—exemplified by hCG—drive the decidual program and sustain developmental progression.

DISCUSSION

Here, we present a 3D human embryo-endometrial co-culture system that robustly recapitulates bidirectional maternal-fetal crosstalk during early post-implantation development. Our platform uniquely supports extended blastocyst development through d.p.f. 14 with high molecular and structural fidelity to *in vivo* CS benchmarks. Critically, it captures emergent hallmarks of early post-implantation stage development, bridging a long-standing gap between isolated embryo models and the physiological maternal niche.

The co-culture system markedly outperforms solo-culture and partial co-culture platforms in both efficiency and complexity. Embryo survival at d.p.f. 14 reached 75%, doubling the rate of

(F) UMAP plots illustrating the comparison of three types of EVT in sole embryos and co-cultured embryos at d.p.f. 9, 12, and 14 (no EVT in sole embryos at d.p.f. 9).
(G) The percentage of each cell type of EVT in relation to the total sequenced population for each sample.
(H) Heatmap of differentially expressed genes (DEGs) across the sole embryos and co-cultured embryos. The colors from blue to red indicate relative expression levels from low to high. The colors of the blocks at the bottom and right side of the heatmap represent different groups.

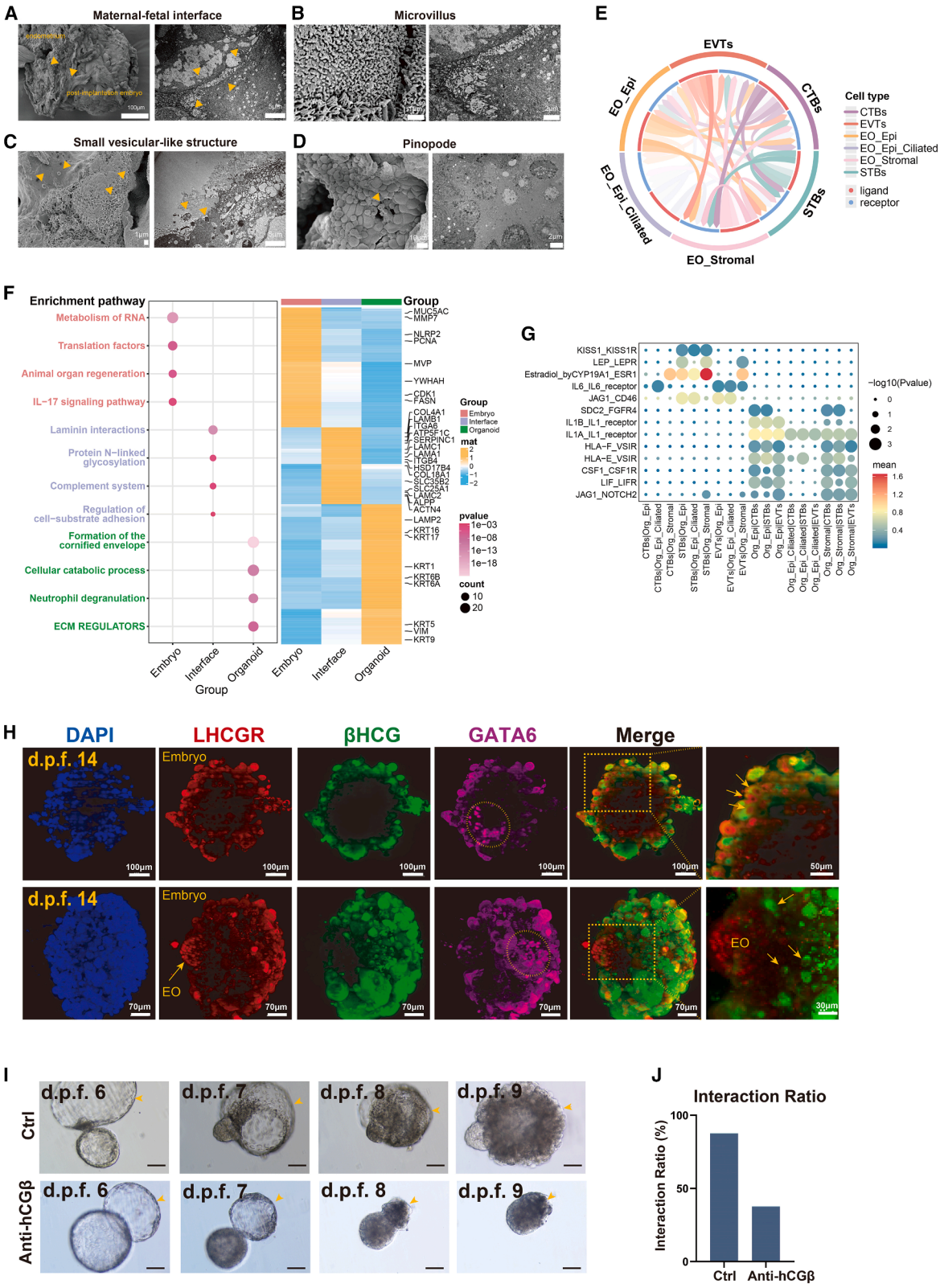

(legend on next page)

embryo-only controls (37.5%) and exceeding reported outcomes in 2D endometrial models (≤50%).[15] Morphometric analyses revealed co-cultured embryos reached diameters of 695.8 ± 64.3 μm, closely aligning with CS7 (700–800 μm) and significantly surpassing solo-cultured counterparts (465.4 ± 129.5 μm). Live imaging further revealed synchronized dynamic remodeling between embryo and endometrium—including cyclical contraction-expansion, polar attachment (81% incidence), and progressive TE invasion—phenomena unobservable in static embryoid models[46] or transwell-based systems.

An important insight is the accelerated emergence of functional HLA-G⁺ EVTs at d.p.f. 9, 3 days earlier than observed in solo cultures and unreported in embryoids or partial co-cultures.[15,47] Single-cell transcriptomics and immunofluorescence confirmed these early iEVTs expressed invasive signatures (*ITGA2*, *MMP9*, and *IL6*) and exhibited enrichment in IL-17/TNF pathways, recapitulating molecular hallmarks of placental bed colonization. While TE organoids have modeled aspects of EVT specification, they lack embryonic context. Our data demonstrate that endometrial cues reprogram TE trajectories, accelerating the EVT1 → EVT2 → iEVT transition and providing the first direct functional evidence that maternal tissue actively instructs EVT maturation. Given that the HIVC medium sustaining the co-culture of human embryos and EOs contains human serum—unlike the fetal-bovine serum used in the embryo-only studies we cite—the enhanced TE maturation observed in our 3D post-implantation system is a combined outcome of both the human-specific nutritional milieu and the instructive presence of the endometrial tissue.

Functional interrogation of hCG-LHCGR signaling revealed it as a keystone of embryo-maternal dialogue. Immunostaining confirmed perinuclear LHCGR localization in β-hCG⁺ STBs, consistent with autocrine/paracrine regulation. hCG neutralization abolished embryo adhesion at d.p.f. 6 (0% versus 50% in controls) and arrested development beyond d.p.f. 9, providing mechanistic support for hCG's clinical role as a biomarker of pregnancy viability.[48] These findings offer a translational framework for understanding recurrent miscarriage and infertility disorders linked to impaired implantation.

All experiments were conducted in strict accordance with Chinese national policies and international ethical guidelines, including the 2003 Human Embryonic Stem Cell Research Ethics Guidelines and the 2021 International Society for Stem Cell Research (ISSCR) Guidelines for Stem Cell Research and Clinical Translation. Embryo culture was terminated by ≤13.5 d.p.f., in compliance with the 14-day rule and without intrauterine culture. Research protocols were approved by the Ethics Committee of the Center for Reproductive Medicine at Shandong University ([2021] ER #14) and the institutional review board (IRB) of Qilu Hospital (KYLL-202204-030), following rigorous scientific and ethical review. Informed consent was obtained from all donors without financial inducement, and all sample use was transparently disclosed.

In summary, our co-culture system establishes an *in vitro* human embryo-maternal unit. By surpassing 2D systems in developmental fidelity, transcending embryoids in physiological relevance, and uncovering instructive roles for endometrial cues and hCG-mediated signaling, this platform offers a transformative foundation for dissecting early implantation biology. Its versatility enables mechanistic exploration of implantation failure, pregnancy loss, and placental dysfunction.

Limitations of the study

Our model, while advancing the field, faces several inherent limitations. First, the physiological simplification of the endometrial niche imposes key constraints. The absence of vascularization precludes eEVT differentiation and systemic nutrient-waste exchange, while the reversed polarity of EOs (apical-in) prevents faithful recapitulation of early steps of implantation. Second, technical hurdles in three-dimensional spatial phenotyping remain. Whole-mount imaging of large co-cultures (600–800 μm) requires Matrigel removal and tissue clearing, which risks damaging delicate cavities during permeabilization—representing a trade-off between molecular resolution and structural integrity. Third, the intrinsic scarcity of human embryos limits both cohort size and mechanistic depth. Biological heterogeneity, including divergent developmental tempo and lineage asynchrony (e.g., delayed EPI progression[49]), is magnified in small cohorts and complicates generalization. These limitations underscore not only the ethical imperatives but also the biological complexities of modeling human embryogenesis. Future integration of vascularized endometrial constructs via 3D bioprinting, microfluidic metabolite regulation, and stem cell-derived embryo models[50] offers a path to overcome these constraints. This post-implantation survival platform enables molecular dissection of TE-endometrium crosstalk *in vivo*. It is not a full replica of the uterus. Instead, it provides an experimentally tractable model for investigating how the human

Figure 6. HCG-LHCGR signaling and vesicle-mediated interactions mediate embryo adhesion

(A–D) Representative scanning electron micrographs of maternal-fetal interface[30] at d.p.f. 12 (scale bar, 100 and 5 μm) (A), showing the microvillus[31–33] (scale bar, 1 and 2 μm) (B), and pinopodes[34] (scale bar, 10 and 2 μm) (C), small vesicular structures[30] (scale bar, 1 and 5 μm) (D). Yellow arrows indicate the location of the endometrium and embryo (A), vesicle (B), and pinopodes (D) in the maternal-fetal interface.

(E) Circle plot displaying the receptor-ligand interactions between EO and TE using scRNA-seq data.

(F) The left bubble chart displays the enriched pathways from SP analysis of a d.p.f. 9 co-cultured embryo. The right heatmap shows the gene expression profiles corresponding to the enriched pathways. The size of the dot represents the gene counts, while the color indicates the *p* value. The color of the heatmap reflects the expression levels of the related genes.

(G) Bubble diagram displaying the representative receptor-ligand between EO and TE. The size of the dot represents the *p* value. The color of the dot indicates the expression level of receptor-ligand pairs.

(H) Whole-mount IF staining demonstrated the expression of βhCG and its receptor LHCGR in the embryo-EO co-culture system at d.p.f. 14. Scale bars (top row), 100 and 50 μm (magnification). Scale bars (bottom row), 70 μm and 30 μm (magnification). In the magnified image, the yellow arrow indicates the syncytiotrophoblast cells of βhCG⁺ LHCGR⁺.

(I) Bright-field images showing the developmental status from d.p.f. 6 to 9 of human embryos in the hCGβ antibody group and the control group. Scale bar, 100 μm.

(J) Interaction ratio of d.p.f. 9 human embryos in the hCGβ antibody group (37.5%, *n* = 8) and the control group (87.5%, *n* = 8).s

embryo survives and develops during the first days after implantation *in vivo* and for decoding the embryo-maternal microenvironmental signaling that underpins this process.

RESOURCE AVAILABILITY

Lead contact

Further information and requests for resources and reagents should be directed to and will be fulfilled by the lead contact, Han Zhao (hanzh80@sdu.edu.cn).

Materials availability

This study did not generate any unique reagents. All materials generated in this study can be made available. EOs generated in this study can be made available on request but will require permission and a completed materials transfer agreement from Shandong University.

Data and code availability

- Single-cell RNA-seq data have been deposited at the Genome Sequence Archive (GSA) and are publicly available as of the date of publication. Accession number is listed in the key resources table (GSA: HRA006892). Microscopy data reported in this paper will be shared by the lead contact upon request. The mass spectrometry proteomics data have been deposited to the ProteomeXchange Consortium via the PRIDE[51] partner repository with the dataset identifier PRIDE: PXD067943. All data are available as of the date of publication.
- This paper does not report any original code or algorithms.
- Any additional information required to reanalyze the data reported in this paper is available from the lead contact upon request.

ACKNOWLEDGMENTS

This work was supported by the National Natural Science Foundation of China (82192874 and 82401947), the Excellence Research Group Program of NSFC (32588201), the National Key Research and Development Program of China (2023YFC2705801, 2025YFC3409000, 2024YFC3405600, and 2023YFA1801803), the Innovation Platform for Academicians of Hainan Province (YSPTZX202310), the Shandong Provincial Key Research and Development Program (2024CXPT081), and the Fundamental Research Funds of Shandong University (2023QNTD004). J. Wu is a New York Stem Cell Foundation (NYSCF) Robertson Investigator and Virginia Murchison Linthicum Scholar in Medical Research and is funded by NYSCF and the Discovery and Innovation Grant from the American Society for Reproductive Medicine (ASRM) Research Institute. We sincerely appreciate Prof. Guangdun Peng (Chinese Academy of Sciences), Prof. Ying Zhang (Beijing Normal University), Yongcun Qu (Capital Institute of Physical Education), and Lizhong Liu (University of Texas Southwestern Medical Center) for their insightful comments and discussions. We thank Qianqian Feng and Dan Zhang (Core Facility of Center of Biomedical Analysis, Tsinghua University) for technical support with light-sheet microscopy and data analysis. We thank Boqin Li and Zheng Li (ShanDong Weiya Bio Co., LTD) for assistance with SEM imaging. We are grateful to Lihong Cui and Chenguang Zhao (Center of Biomedical Analysis, Tsinghua University) for assisting with transmission electron microscope imaging. We also thank Nanjing Singleron Biotechnology Company and Novoprotein Scientific Inc. for technical support and Jingjie PTM Biolab (HangZhou) Co., Inc. for organoid medium and proteomics. We thank Prof. Wei Xie (Tsinghua University), Prof. Xukun Lu (Shandong University), Prof. Tianqing Li (Kunming University of Science and Technology), Prof. Yu Yin (Kunming University of Science and Technology), Prof. Huili Hu (Shandong University), and Prof. Lifeng Xiang (The First People's Hospital of Yunnan Province) for discussion and comments during the preparation of the manuscript.

AUTHOR CONTRIBUTIONS

H.Z., Z.-J.C., and K.W. initiated, sponsored, and supervised the entire project. J. Wu guided the study and revised the manuscript. J.S., R.Z., and Y.Z. jointly constructed and optimized the co-culture system. J.S. performed embryo culture, single-cell isolation, scRNA-seq library preparation, embryonic morphology experiments, video production, and drafting of the manuscript. R.Z. performed embryonic morphology experiments, image processing, 3D reconstruction, video production, data analysis, and drafting of the manuscript. Y.Z. established receptive EOs, performed organoid-embryo immunofluorescence, produced 3D video of organoids, and drafted and revised the manuscript. M.L. and Y.H. cultured the EOs. R.Z., H.Y., X.C., Y.Z., X.Z., Y.S., R.Y., Y.H., Z.H., and M.L. assisted *in vitro* embryo culture experiments. C.L., W.T., and J.Z. prepared donated human IVF embryos and provided technical support for *in vitro* culture. P.L. and T.L. provided a human endometrium sample. D.S. and Q.Z. assisted with data analysis. J.S., Y.Z., H.Y., X.C., Z.H., W.T., and J.Z. together were responsible for the digestion and dissociation of embryos and the collection of single cells. H.Y., Z.H., and J. Wang helped with whole-mount clearing and immunofluorescence. W.L. and X.G. conducted the image processing and video production. R.Y. and Y.S. provided technical support. Y.Q. and H.W. contributed critically to the project design. H.Z. and J. Wu revised the manuscript with inputs from all authors.

DECLARATION OF INTERESTS

The authors declare no competing interests.

STAR★METHODS

Detailed methods are provided in the online version of this paper and include the following:

- KEY RESOURCES TABLE
- EXPERIMENTAL MODEL AND STUDY PARTICIPANT DETAILS
  - Ethics statement
  - Human samples
- METHOD DETAILS
  - Human embryo thawing
  - Establishment of endometrial organoids
  - Hormone treatment of endometrial organoids
  - Embryo-endometrium co-culture
  - Toluidine Staining
  - Sample clearing, immunostaining and image analysis
  - Transmission electron microscopy (TEM) and Scanning electronic microscopy (SEM)
  - Single-cell library preparation and sequencing
  - Quality control, dimension-reduction and clustering
  - Differentially expressed genes (DEGs) analysis
  - Cell-cell communication analysis
  - Pseudotime construction
  - Comparison analysis with published available datasets
  - Batch correction
  - Spatial proteomics

SUPPLEMENTAL INFORMATION

Supplemental information can be found online at https://doi.org/10.1016/j.stem.2025.12.002.

Received: December 18, 2024
Revised: September 2, 2025
Accepted: December 2, 2025
Published: December 23, 2025

REFERENCES

1. Molè, M.A., Weberling, A., Fässler, R., Campbell, A., Fishel, S., and Zernicka-Goetz, M. (2021). Integrin β1 coordinates survival and morphogenesis of the embryonic lineage upon implantation and pluripotency transition. Cell Rep. *34*, 108834. https://doi.org/10.1016/j.celrep.2021.108834.
2. Cha, J., Sun, X., and Dey, S.K. (2012). Mechanisms of implantation: strategies for successful pregnancy. Nat. Med. *18*, 1754–1767. https://doi.org/10.1038/nm.3012.

3. Biase, F.H., Hue, I., Dickinson, S.E., Jaffrezic, F., Laloe, D., Lewin, H.A., and Sandra, O. (2019). Fine-tuned adaptation of embryo–endometrium pairs at implantation revealed by transcriptome analyses in Bos taurus. PLoS Biol. *17*, e3000046. https://doi.org/10.1371/journal.pbio.3000046.

4. Xiang, L., Yin, Y., Zheng, Y., Ma, Y., Li, Y., Zhao, Z., Guo, J., Ai, Z., Niu, Y., Duan, K., et al. (2020). A developmental landscape of 3D-cultured human pre-gastrulation embryos. Nature *577*, 537–542. https://doi.org/10.1038/s41586-019-1875-y.

5. Shahbazi, M.N., Jedrusik, A., Vuoristo, S., Recher, G., Hupalowska, A., Bolton, V., Fogarty, N.N.M., Campbell, A., Devito, L.G., Ilic, D., et al. (2016). Self-organization of the human embryo in the absence of maternal tissues. Nat. Cell Biol. *18*, 700–708. https://doi.org/10.1038/ncb3347.

6. Deglincerti, A., Croft, G.F., Pietila, L.N., Zernicka-Goetz, M., Siggia, E.D., and Brivanlou, A.H. (2016). Self-organization of the in vitro attached human embryo. Nature *533*, 251–254. https://doi.org/10.1038/nature17948.

7. Zhou, F., Wang, R., Yuan, P., Ren, Y., Mao, Y., Li, R., Lian, Y., Li, J., Wen, L., Yan, L., et al. (2019). Reconstituting the transcriptome and DNA methylome landscapes of human implantation. Nature *572*, 660–664. https://doi.org/10.1038/s41586-019-1500-0.

8. Yu, L., Wei, Y., Duan, J., Schmitz, D.A., Sakurai, M., Wang, L., Wang, K., Zhao, S., Hon, G.C., and Wu, J. (2021). Blastocyst-like structures generated from human pluripotent stem cells. Nature *591*, 620–626. https://doi.org/10.1038/s41586-021-03356-y.

9. Weatherbee, B.A.T., Gantner, C.W., Iwamoto-Stohl, L.K., Daza, R.M., Hamazaki, N., Shendure, J., and Zernicka-Goetz, M. (2023). Pluripotent stem cell-derived model of the post-implantation human embryo. Nature *622*, 584–593. https://doi.org/10.1038/s41586-023-06368-y.

10. Oldak, B., Wildschutz, E., Bondarenko, V., Comar, M.Y., Zhao, C., Aguilera-Castrejon, A., Tarazi, S., Viukov, S., Pham, T.X.A., Ashouokhi, S., et al. (2023). Complete human day 14 post-implantation embryo models from naive ES cells. Nature *622*, 562–573. https://doi.org/10.1038/s41586-023-06604-5.

11. Pedroza, M., Gassaloglu, S.I., Dias, N., Zhong, L., Hou, T.J., Kretzmer, H., Smith, Z.D., and Sozen, B. (2023). Self-patterning of human stem cells into post-implantation lineages. Nature *622*, 574–583. https://doi.org/10.1038/s41586-023-06354-4.

12. Liu, L., Oura, S., Markham, Z., Hamilton, J.N., Skory, R.M., Li, L., Sakurai, M., Wang, L., Pinzon-Arteaga, C.A., Plachta, N., et al. (2023). Modeling post-implantation stages of human development into early organogenesis with stem-cell-derived peri-gastruloids. Cell *186*, 3776–3792.e16. https://doi.org/10.1016/j.cell.2023.07.018.

13. Oura, S., Li, L., and Wu, J. (2025). An inducible model of human post-implantation development derived from primed and naive stem cells. Cell Stem Cell *32*, 1509–1527.e9. https://doi.org/10.1016/j.stem.2025.08.005.

14. Liu, D., Chen, Y., Ren, Y., Yuan, P., Wang, N., Liu, Q., Yang, C., Yan, Z., Yang, M., Wang, J., et al. (2022). Primary specification of blastocyst trophectoderm by scRNA-seq: New insights into embryo implantation. Sci. Adv. *8*, eabj3725. https://doi.org/10.1126/sciadv.abj3725.

15. Yu, L., Logsdon, D., Pinzon-Arteaga, C.A., Duan, J., Ezashi, T., Wei, Y., Ribeiro Orsi, A.E., Oura, S., Liu, L., Wang, L., et al. (2023). Large-scale production of human blastoids amenable to modeling blastocyst development and maternal-fetal cross talk. Cell Stem Cell *30*, 1246–1261.e9. https://doi.org/10.1016/j.stem.2023.08.002.

16. Zhang, Y., Zhao, R., Yang, C., Song, J., Liu, P., Li, Y., Liu, B., Li, T., Yin, C., Lu, M., et al. (2024). Human receptive endometrial organoid for deciphering the implantation window. eLife *13*, RP93873. https://doi.org/10.7554/eLife.93873.

17. Tian, J., Yang, J., Chen, T., Yin, Y., Li, N., Li, Y., Luo, X., Dong, E., Tan, H., Ma, Y., et al. (2023). Generation of Human Endometrial Assembloids with a Luminal Epithelium using Air-Liquid Interface Culture Methods. Adv. Sci. (Weinh) *10*, e2301868. https://doi.org/10.1002/advs.202301868.

18. Hertig, A.T., and Rock, J. (1945). Two human ova of the pre-villous stage, having a developmental age of about seven and nine days respectively. Carnegie Inst. Wash. Publ. 575, Contrib. Embryol. *35*, 67–84.

19. Hertig, A.T. (1945). On the development of the amnion and exoccelomic membrane in the previllous human ovum. Yale J. Biol. Med. *18*, 107–115.

20. Hertig, A.T., and Rock, J. (1941). Two human ova of the pre-villous stage, having an ovulation age of about eleven and twelve days respectively. Carnegie Inst. Wash. Publ. 557, Contrib. Embryol. *29*, 127–156.

21. Heuser, C.H., Rock, J., and Hertig, A.T. (1945). Two human embryos showing early stages of the definitive yolk sac. Carnegie Inst. Wash. Publ. 557. Contrib. Embryol. *31*, 85–99.

22. Irie, N., Weinberger, L., Tang, W.W.C., Kobayashi, T., Viukov, S., Manor, Y.S., Dietmann, S., Hanna, J.H., and Surani, M.A. (2015). SOX17 is a critical specifier of human primordial germ cell fate. Cell *160*, 253–268. https://doi.org/10.1016/j.cell.2014.12.013.

23. Ma, H., Zhai, J., Wan, H., Jiang, X., Wang, X., Wang, L., Xiang, Y., He, X., Zhao, Z.A., Zhao, B., et al. (2019). In vitro culture of cynomolgus monkey embryos beyond early gastrulation. Science *366*, eaax7890. https://doi.org/10.1126/science.aax7890.

24. Hertig, A.T., and Rock, J. (1944). On the development of the early human ovum, with special reference to the trophoblast of the previllous stage: A desoription of 7 normal and 5 pathologic human ova. Am. J. Obstet. Gynecol. *47*, 149–184. https://doi.org/10.1016/S0002-9378(44)90252-8.

25. Zhang, S., Lin, H., Kong, S., Wang, S., Wang, H., Wang, H., and Armant, D.R. (2013). Physiological and molecular determinants of embryo implantation. Mol. Aspects Med. *34*, 939–980. https://doi.org/10.1016/j.mam.2012.12.011.

26. Arutyunyan, A., Roberts, K., Troulé, K., Wong, F.C.K., Sheridan, M.A., Kats, I., Garcia-Alonso, L., Velten, B., Hoo, R., Ruiz-Morales, E.R., et al. (2023). Spatial multiomics map of trophoblast development in early pregnancy. Nature *616*, 143–151. https://doi.org/10.1038/s41586-023-05869-0.

27. Jaremek, A., Jeyarajah, M.J., Jaju Bhattad, G., and Renaud, S.J. (2021). Omics Approaches to Study Formation and Function of Human Placental Syncytiotrophoblast. Front. Cell Dev. Biol. *9*, 674162. https://doi.org/10.3389/fcell.2021.674162.

28. Adiguzel, D., and Celik-Ozenci, C. (2021). FoxO1 is a cell-specific core transcription factor for endometrial remodeling and homeostasis during menstrual cycle and early pregnancy. Hum. Reprod. Update *27*, 570–583. https://doi.org/10.1093/humupd/dmaa060.

29. Marinić, M., Mika, K., Chigurupati, S., and Lynch, V.J. (2021). Evolutionary transcriptomics implicates HAND2 in the origins of implantation and regulation of gestation length. eLife *10*, e61257. https://doi.org/10.7554/eLife.61257.

30. Liu, Y., Kodithuwakku, S.P., Ng, P.Y., Chai, J., Ng, E.H.Y., Yeung, W.S.B., Ho, P.C., and Lee, K.F. (2010). Excessive ovarian stimulation up-regulates the Wnt-signaling molecule DKK1 in human endometrium and may affect implantation: an in vitro co-culture study. Hum. Reprod. *25*, 479–490. https://doi.org/10.1093/humrep/dep429.

31. Sabine, V.S., Faratian, D., Kirkegaard-Clausen, T., and Bartlett, J.M.S. (2012). Validation of activated caspase-3 antibody staining as a marker of apoptosis in breast cancer. Histopathology *60*, 369–371. https://doi.org/10.1111/j.1365-2559.2011.04024.x.

32. Heaton, H., Talman, A.M., Knights, A., Imaz, M., Gaffney, D.J., Durbin, R., Hemberg, M., and Lawniczak, M.K.N. (2020). Souporcell: robust clustering of single-cell RNA-seq data by genotype without reference genotypes. Nat. Methods *17*, 615–620. https://doi.org/10.1038/s41592-020-0820-1.

33. Tyser, R.C.V., Mahammadov, E., Nakanoh, S., Vallier, L., Scialdone, A., and Srinivas, S. (2021). Single-cell transcriptomic characterization of a gastrulating human embryo. Nature *600*, 285–289. https://doi.org/10.1038/s41586-021-04158-y.

34. Li, Q., Sharkey, A., Sheridan, M., Magistrati, E., Arutyunyan, A., Huhn, O., Sancho-Serra, C., Anderson, H., McGovern, N., Esposito, L., et al. (2024). Human uterine natural killer cells regulate differentiation of extravillous trophoblast early in pregnancy. Cell Stem Cell *31*, 181–195.e9. https://doi.org/10.1016/j.stem.2023.12.013.

35. Mincheva-Nilsson, L. (2021). Immunosuppressive Protein Signatures Carried by Syncytiotrophoblast-Derived Exosomes and Their Role in Human Pregnancy. Front. Immunol. *12*, 717884. https://doi.org/10.3389/fimmu.2021.717884.

36. McConkey, C.A., Delorme-Axford, E., Nickerson, C.A., Kim, K.S., Sadovsky, Y., Boyle, J.P., and Coyne, C.B. (2016). A three-dimensional culture system recapitulates placental syncytiotrophoblast development and microbial resistance. Sci. Adv. *2*, e1501462. https://doi.org/10.1126/sciadv.1501462.

37. Cao, R., Wang, Y., Liu, J., Rong, L., and Qin, J. (2023). Self-assembled human placental model from trophoblast stem cells in a dynamic organ-on-a-chip system. Cell Prolif. *56*, e13469. https://doi.org/10.1111/cpr.13469.

38. Io, S., Kabata, M., Iemura, Y., Semi, K., Morone, N., Minagawa, A., Wang, B., Okamoto, I., Nakamura, T., Kojima, Y., et al. (2021). Capturing human trophoblast development with naive pluripotent stem cells in vitro. Cell Stem Cell *28*, 1023–1039.e13. https://doi.org/10.1016/j.stem.2021.03.013.

39. Melkozerova, O., Shchedrina, I., Gryshkina, A., Bashmakova, N., Malgina, G., Michelson, A., and Chistyakova, G. (2020). How noninvasive treatment of uterine fibroids affects endometrial receptivity: a prospective cohort study. Gynecol. Endocrinol. *36*, 28–32. https://doi.org/10.1080/09513590.2020.1816725.

40. Massuto, D.A., Kneese, E.C., Johnson, G.A., Burghardt, R.C., Hooper, R.N., Ing, N.H., and Jaeger, L.A. (2010). Transforming growth factor beta (TGFB) signaling is activated during porcine implantation: proposed role for latency-associated peptide interactions with integrins at the conceptus-maternal interface. Reproduction *139*, 465–478. https://doi.org/10.1530/rep-09-0447.

41. Miner, J.H., Li, C., Mudd, J.L., Go, G., and Sutherland, A.E. (2004). Compositional and structural requirements for laminin and basement membranes during mouse embryo implantation and gastrulation. Development *131*, 2247–2256. https://doi.org/10.1242/dev.01112.

42. Dey, S.K., Lim, H., Das, S.K., Reese, J., Paria, B.C., Daikoku, T., and Wang, H. (2004). Molecular cues to implantation. Endocr. Rev. *25*, 341–373. https://doi.org/10.1210/er.2003-0020.

43. Chen, R., Fan, R., Chen, F., Govindasamy, N., Brinkmann, H., Stehling, M., Adams, R.H., Jeong, H.W., and Bedzhov, I. (2024). Analyzing embryo dormancy at single-cell resolution reveals dynamic transcriptional responses and activation of integrin-Yap/Taz prosurvival signaling. Cell Stem Cell *31*, 1262–1279.e8. https://doi.org/10.1016/j.stem.2024.06.015.

44. Qin, L., Wang, Y.L., Bai, S.X., Ji, S.H., Qiu, W., Tang, S., and Piao, Y.S. (2003). Temporal and spatial expression of integrins and their extracellular matrix ligands at the maternal-fetal interface in the rhesus monkey during pregnancy. Biol. Reprod. *69*, 563–571. https://doi.org/10.1095/biolreprod.103.015198.

45. Garcia-Alonso, L., Lorenzi, V., Mazzeo, C.I., Alves-Lopes, J.P., Roberts, K., Sancho-Serra, C., Engelbert, J., Marečková, M., Gruhn, W.H., Botting, R.A., et al. (2022). Single-cell roadmap of human gonadal development. Nature *607*, 540–547. https://doi.org/10.1038/s41586-022-04918-4.

46. Shibata, S., Endo, S., Nagai, L.A.E., H Kobayashi, E., Oike, A., Kobayashi, N., Kitamura, A., Hori, T., Nashimoto, Y., Nakato, R., et al. (2024). Modeling embryo-endometrial interface recapitulating human embryo implantation. Sci. Adv. *10*, eadi4819. https://doi.org/10.1126/sciadv.adi4819.

47. Fujimura, T., Tamura, I., Yoshimura, A., Yoneda, T., Takasaki, H., Shiroshita, A., Shirafuta, Y., Sato, S., and Sugino, N. (2025). Establishment of an in vitro implantation model using a newly developed mouse endometrial organoid. Development *152*, dev204461. https://doi.org/10.1242/dev.204461.

48. Mansour, R., Tawab, N., Kamal, O., El-Faissal, Y., Serour, A., Aboulghar, M., and Serour, G. (2011). Intrauterine injection of human chorionic gonadotropin before embryo transfer significantly improves the implantation and pregnancy rates in in vitro fertilization/intracytoplasmic sperm injection: a prospective randomized study. Fertil. Steril. *96*, 1370–1374.e1. https://doi.org/10.1016/j.fertnstert.2011.09.044.

49. Ministerial Meeting on Population of the Non-Aligned Movement (1993: Bali) (1994). Denpasar Declaration on Population and Development. Integration, 27–29. https://doi.org/10.1234/2013/999990.

50. Wu, J., and Fu, J. (2024). Toward developing human organs via embryo models and chimeras. Cell *187*, 3194–3219. https://doi.org/10.1016/j.cell.2024.05.027.

51. Perez-Riverol, Y., Xu, Q.W., Wang, R., Uszkoreit, J., Griss, J., Sanchez, A., Reisinger, F., Csordas, A., Ternent, T., Del-Toro, N., et al. (2016). PRIDE Inspector Toolsuite: Moving Toward a Universal Visualization Tool for Proteomics Data Standard Formats and Quality Assessment of ProteomeXchange Datasets. Mol. Cell. Proteomics *15*, 305–317. https://doi.org/10.1074/mcp.O115.050229.

52. Ai, Z., Niu, B., Yin, Y., Xiang, L., Shi, G., Duan, K., Wang, S., Hu, Y., Zhang, C., Zhang, C., et al. (2023). Dissecting peri-implantation development using cultured human embryos and embryo-like assembloids. Cell Res. *33*, 661–678. https://doi.org/10.1038/s41422-023-00846-8.

53. Molè, M.A., Coorens, T.H.H., Shahbazi, M.N., Weberling, A., Weatherbee, B.A.T., Gantner, C.W., Sancho-Serra, C., Richardson, L., Drinkwater, A., Syed, N., et al. (2021). A single cell characterisation of human embryogenesis identifies pluripotency transitions and putative anterior hypoblast centre. Nat. Commun. *12*, 3679. https://doi.org/10.1038/s41467-021-23758-w.

54. Wolf, F.A., Angerer, P., and Theis, F.J. (2018). SCANPY: large-scale single-cell gene expression data analysis. Genome Biol. *19*, 15. https://doi.org/10.1186/s13059-017-1382-0.

55. Murakami, T.C., Mano, T., Saikawa, S., Horiguchi, S.A., Shigeta, D., Baba, K., Sekiya, H., Shimizu, Y., Tanaka, K.F., Kiyonari, H., et al. (2018). A three-dimensional single-cell-resolution whole-brain atlas using CUBIC-X expansion microscopy and tissue clearing. Nat. Neurosci. *21*, 625–637. https://doi.org/10.1038/s41593-018-0109-1.

56. Picelli, S., Faridani, O.R., Björklund, A.K., Winberg, G., Sagasser, S., and Sandberg, R. (2014). Full-length RNA-seq from single cells using Smart-seq2. Nat. Protoc. *9*, 171–181. https://doi.org/10.1038/nprot.2014.006.

57. Qiu, X., Hill, A., Packer, J., Lin, D., Ma, Y.A., and Trapnell, C. (2017). Single-cell mRNA quantification and differential analysis with Census. Nat. Methods *14*, 309–315. https://doi.org/10.1038/nmeth.4150.

58. Stuart, T., Srivastava, A., Madad, S., Lareau, C.A., and Satija, R. (2021). Single-cell chromatin state analysis with Signac. Nat. Methods *18*, 1333–1341. https://doi.org/10.1038/s41592-021-01282-5.

59. Haghverdi, L., Büttner, M., Wolf, F.A., Buettner, F., and Theis, F.J. (2016). Diffusion pseudotime robustly reconstructs lineage branching. Nat. Methods *13*, 845–848. https://doi.org/10.1038/nmeth.3971.

60. Xu, C., Prete, M., Webb, S., Jardine, L., Stewart, B.J., Hoo, R., He, P., Meyer, K.B., and Teichmann, S.A. (2023). Automatic cell-type harmonization and integration across Human Cell Atlas datasets. Cell *186*, 5876–5891.e20. https://doi.org/10.1016/j.cell.2023.11.026.

61. Yu, G., Wang, L.G., Han, Y., and He, Q.Y. (2012). clusterProfiler: an R package for comparing biological themes among gene clusters. OMICS *16*, 284–287. https://doi.org/10.1089/omi.2011.0118.

STAR★METHODS

KEY RESOURCES TABLE

REAGENT or RESOURCE	SOURCE	IDENTIFIER
Antibodies		
Mouse anti-Oct3/4(clone C-10)	Santa Cruz	Cat# SC-5279; RRID: AB_628051
Goat anti-Sox17	R&D Systems	Cat# AF1924; RRID: AB_355060
Goat anti-Gata3	R&D Systems	Cat# AF2605; RRID: AB_2108571
Rabbit anti-SDC-1	Abcam	Cat# ab128936; RRID: AB_11150990
Rabbit anti-Brachyury (D2Z3J)	Cell Signaling	Cat# 81694; RRID: AB_2799983
Goat anti-Cer1	R&D Systems	Cat# AF1075; RRID: AB_2077228
Rabbit anti-Vimentin	Cell Signaling	Cat# 5741; RRID: AB_10695459
Rabbit anti-hCG beta (5H4-E2)	Abcam	Cat# ab9582; RRID: AB_296507
Rabbit anti-Islet1(EP4182)	Abcam	Cat# ab109517; RRID: AB_10866454
Mouse anti-TFAP2a(AP-2α) (3B5)	Santa Cruz	Cat# SC-12726; RRID: AB_667767
Goat anti-Sox2	R&D Systems	Cat# AF2018; RRID: AB_355110
Rabbit anti-Blimp1/PDRI-BF1 (clone C14A4)	Cell Signaling	Cat# 9115; RRID: AB_2169699
Mouse anti-Cytokeratin 7	Dako	Cat# M7018; RRID: AB_2134589
Goat anti-GATA6	R&D Systems	Cat# AF1700; RRID: AB_2108901
Mouse anti-Estrogen Receptor alpha	Santa Cruz	Cat# sc-8002; RRID: AB_627558
Mouse anti-FoxO1(D7C1H)	Cell Signaling	Cat# 14952; RRID: AB_2722487
Rabbit anti-Progesterone Receptor A/B (D8Q2J) XP®	Cell Signaling	Cat# 8757; RRID: AB_2797144
Rabbit anti-Rabbit anti-FOXA2	Abcam	Cat# ab108422; RRID: AB_11157157
Mouse anti-WNT7A	Santa Cruz	Cat# sc-365665; RRID: AB_10846318
CD45 Monoclonal Antibody (30-F11)	ThermoFisher	Cat# 14-0451-81; RRID: AB_467250
Rabbit anti-HAND2[EPR19451]	Abcam	Cat# ab200040; RRID: AB_2923502
Rabbit anti-DKK1 (D5V6L)	Cell Signaling	Cat# 48367; RRID: AB_2799337
Mouse anti-Ki-67(8D5)	Cell Signaling	Cat# 9449; RRID: AB_2797703
Rabbit anti-Cleaved Caspase-3 (Asp175)	Cell Signaling	Cat# 9661; RRID: AB_2341188
LHCGR Polyclonal antibody	Proteintech	Cat# 19968-1-AP; RRID: AB_10697685
βHCG	ThermoFisher	Cat# MA1-35020; RRID: AB_1073663
Alexa Fluor™ 488 phalloidin	ThermoFisher	Cat# A12379
Phalloidin Labeling Probes	ThermoFisher	Cat# A30104
Anti-HLA G	Abcam	Cat# AB283260; RRID: AB_2924400
TEAD4	Atlas Antibodies	Cat# HPA056896; RRID: AB_2683268
Human Otx2 Antibody	R&D	Cat# AF1979; RRID: AB_2157172
Donkey anti-Mouse IgG (H+L) Highly Cross-Adsorbed Secondary Antibody Alexa Fluor™ Plus 488	ThermoFisher	Cat# A32766; RRID: AB_2762823
Donkey anti-Mouse IgG (H+L) Highly Cross-Adsorbed Secondary Antibody Alexa Fluor™ Plus 555	ThermoFisher	Cat# A32773; RRID: AB_2762848
Donkey anti-Rabbit IgG (H+L) Highly Cross-Adsorbed Secondary Antibody Alexa Fluor™ Plus 555	ThermoFisher	Cat# A32794; RRID: AB_2762834
Donkey anti-Rabbit IgG (H+L) Highly Cross-Adsorbed Secondary Antibody Alexa Fluor™ Plus 488	ThermoFisher	Cat# A32790; RRID: AB_2762833

(*Continued on next page*)

Continued

REAGENT or RESOURCE	SOURCE	IDENTIFIER
Donkey anti-Rabbit IgG (H+L) Highly Cross-Adsorbed Secondary Antibody Alexa Fluor™ Plus 647	ThermoFisher	Cat# A32795; RRID: AB_2762835
Donkey anti-Goat IgG (H+L) Highly Cross-Adsorbed Secondary Antibody Alexa Fluor™ Plus 647	ThermoFisher	Cat# A32849; RRID: AB_2762840
Donkey anti-Rabbit IgG (H+L) Highly Cross-Adsorbed Secondary Antibody, Alexa Fluor™ 488	ThermoFisher	Cat# A21206; RRID: AB_2535792
Donkey anti-Rabbit IgG (H+L) Highly Cross-Adsorbed Secondary Antibody, Alexa Fluor™ 555	ThermoFisher	Cat# A31572; RRID: AB_162543
Donkey anti-Rabbit IgG (H+L) Highly Cross-Adsorbed Secondary Antibody, Alexa Fluor™ 647	ThermoFisher	Cat# A31573; RRID: AB_162543?
Donkey anti-Mouse IgG (H+L) Highly Cross-Adsorbed Secondary Antibody, Alexa Fluor™ 488	ThermoFisher	Cat# A21202; RRID: AB_141607
Donkey anti-Mouse IgG (H+L) Highly Cross-Adsorbed Secondary Antibody, Alexa Fluor™ 555	ThermoFisher	Cat# A31570; RRID: AB_2536180
Donkey anti-Mouse IgG (H+L) Highly Cross-Adsorbed Secondary Antibody, Alexa Fluor™ 647	ThermoFisher	Cat# A31571; RRID: AB_162542
Donkey anti-Goat IgG (H+L) Cross-Adsorbed Secondary Antibody, Alexa Fluor™ 488	ThermoFisher	Cat# A11055; RRID: AB_2534102
Donkey anti-Goat IgG (H+L) Cross-Adsorbed Secondary Antibody, Alexa Fluor™ 555	ThermoFisher	Cat# A21432; RRID: AB_253583
Donkey anti-Goat IgG (H+L) Cross-Adsorbed Secondary Antibody, Alexa Fluor™ 647	ThermoFisher	Cat# A21447; RRID: AB_2535864
Chemicals, peptides, and recombinant proteins		
DMEM/F12	Gibco	11039-021
Antibiotic-Antimycotic (100X)	Gibco	15240062
ITS	Gibco	41400-045
L-Glutamine	Gibco	25030-081
Nicotinamide	Sigma	N3376
B27	Gibco	17504-044
N2	Gibco	17502-048
Noggin	Proteintech	HZ-1118
EGF	Peprotech	AF-100-15
FGF2	Origene	TP750002
WNT-3A	Proteintech	HZ-1296
R-Spondin-1	Peprotech	120-38
A83-01	MCE	HY-10432
N-acetyl-L-cysteine	Sigma	A7250
p38 inhibitor SB202190	Sigma	SB202190
Estradiol	Sigma	E2758
Medroxyprogesterone Acetate	Selleck	S2567
N6,2′-O-dibutyryladenosine 3′,5′-cyclic monophosphate sodium salt (cAMP)	Sigma	D0627
Human Chorionic Gonadotropin (HCG)	Livzon Pharmaceutical Group Inc	2000U
Human Placental Lactogen (HPL)	R&D Systems	5757-PL
Prolactin	Peprotech	100-07
Advanced DMEM/F12	Gibco	12634-010
GlutaMAX	Thermo Fisher Scientific	35050-038
ITS-X	Thermo Fisher Scientific	51500-056
Penicillin–streptomycin	Gibco	15070063
HBS	Sigma-Aldrich	H3667 or H5667

(*Continued on next page*)

Continued

REAGENT or RESOURCE	SOURCE	IDENTIFIER
sodium lactate	Sigma-Aldrich	L7900
sodium pyruvate (500 mM stock)	Sigma-Aldrich	P4562
β-Estradiol (8 μM stock)	Sigma-Aldrich	E8875-1G
Y27632(10 mM stock)	Selleck	S1049
Progesterone (2 mg/ml stock)	Sigma-Aldrich	P8783-1G
NAC (250 mM stock)	Sigma-Aldrich	A7250
Matrigel	Corning	354234
Critical commercial assays		
Tissue-Clearing Reagent CUBIC-L	tcichemicals	T3740
Tissue-Clearing Reagent CUBIC-R+(M)	tcichemicals	T3741
Experimental models: Cell lines		
Endometrial organoid	Han Zhao et al.[16]	N/A
Deposited data		
scRNA-seq (GEXSCOPE®&10X) of d.p.f. 9, 12, 14 embryos and EOs	This study	GSA: HRA006892
scRNA-seq (Smart-seq2) of d.p.f. 14 embryos and Eos	This study	GSA: HRA006892
Spatial proteomics of d.p.f. 9 embryos and Eos	This study	PXD067943
scRNA-seq (10x) of d.p.f 8,10,12,14 embryos	Ai et al.[52]	PRJCA017779
scRNA-seq (10x) of d.p.f 9-11 embryos	Molè et al.[53]	E-MTAB-8060
scRNA-seq (Smart-seq2) of Human gastrulation	Tyser et al.[33]	PRJEB40781
Smart-seq2 of d.p.f. 14 embryos	Xiang et al.[4]	GEO: GSE136447
scRNA-seq (10x) of Endometrial organoids	Zhang et al.[16]	GSA: HRA007224
Software and algorithms		
Imaris x64 (version 10.0.1)	Oxford Instruments	https://imaris.oxinst.com/packages
Scanpy (version1.8.1)	Python Software Foundation	https://scanpy.readthedocs.io/en/stable/
CellPhoneDB(version 4)	Qin et al.[44]	https://github.com/sqjin/CellChat
Monocle2 (version 2.22.)	Wolf et al.[54]	https://github.com/cole-trapnell-lab/
Seurat(version 4.1.0)		https://satijalab.org/seurat/
Harmonypy (version1.0.0)		https://github.com/slowkow/harmonypy
Prism 9	GraphPad	https://www.graphpad.com/
Souporcell (version 2.4)	Heaton et al.[32]	https://github.com/wheaton5/souporcell
UMAP (version 0.5.3)		https://github.com/lmcinnes/umap
DoubletDetection (4.2)	Python Software Foundation	https://pypi.org/project/doubletdetection/
ClusterProfiler (version 4.4.4)		https://bioconductor.org/packages/release/bioc/html/clusterProfiler.html
ComplexHeatmap (version 3.17)		https://bioconductor.org/packages/release/bioc/html/ComplexHeatmap.html
Cell Ranger pipeline (version 6.1.2)	10x Genomics	N/A

EXPERIMENTAL MODEL AND STUDY PARTICIPANT DETAILS

Ethics statement

Human embryo research was conducted with approval from the Ethics Committee of the Center for Reproductive Medicine at Shandong University ([2021] ER #14). This research adheres to the "Management of Human Assisted Reproductive Technology (2001)," "Regulations of Human Assisted Reproductive Technology (2003)," the "Human Biomedical Research Ethics Guidelines" (issued by the National Health Commission of the People's Republic of China on December 1, 2016), the "International Ethical Guidelines for Biomedical Research on Humans" (CIOMS, 2002), the "Guidelines for Stem Cell Research and Clinical Translation" (issued by the International Society for Stem Cell Research, ISSCR, 2021), and the "Human Embryonic Stem Cell Research Ethics Guidelines" (2003) jointly issued by the Ministry of Science and Technology and the Ministry of Health of the People's Republic of China, along with the Helsinki Declaration and other relevant regulations. The Institutional Review Board at the Center for Reproductive Medicine thoroughly assessed both the scientific merit and ethical justification of this study, reviewing the donations and utilization

of samples. All donors provided informed consent for the voluntary donation of surplus embryos, fully understanding that their embryos would be used to investigate post-implantation development *in vitro*. No financial incentives were offered for these donations. The culture of all embryos was terminated either on day 14 post-fertilization or upon the formation of the primitive streak.

Research involving human endometrial organoids was approved by the Institutional Review Board of Qilu Hospital of Shandong University (KYLL-202204-030). All manipulations of human endometrial tissue adhered to the Human Biomedical Research Ethics Guidelines (set by the National Health Commission of the People's Republic of China on December 1, 2016), the International Ethical Guidelines for Biomedical Research on Humans (CIOMS, 2002), the Guidelines for Stem Cell Research and Clinical Translation (ISSCR, 2021), the Helsinki Declaration, and other laws and regulations. The Institutional Review Board comprises 13 members, including lawyers, scientists, and clinicians with relevant expertise. The Committee evaluated the scientific merit and ethical justification of this study and conducted a comprehensive review of the donations and use of these samples. Human endometrium was obtained from women without infertility who underwent hysterectomy due to benign diseases at Qilu Hospital. All donors provided informed consent for the voluntary donation of endometrial tissue, being informed that their samples would be used to explore embryo development processes following the implantation of IVF patients' embryos *in vitro*. No financial inducements were offered for these donations.

Human samples

Human blastocysts were obtained from IVF patients (ages 26-40) without genetic diseases at the Center for Reproductive Medicine, Shandong University, exceeding the clinical needs of the couples. According to the Gardner scoring system, thawed blastocysts were assigned scores from 1 to 6 based on their degree of expansion and hatching status. Only blastocysts with an expansion and hatching score above three and a visible inner cell mass graded higher than B were included in the study. Normal embryos were required to meet two morphological criteria: they needed to exhibit clear expansion during culture and show no evident signs of cell death or fragmentation throughout development. Any embryos not meeting these criteria were excluded from the study.[4]

Human endometrial samples were obtained from nine patients of childbearing age with normal BMI, regular menstrual cycles, and no history of infertility, systemic conditions, or hormonal treatments, who underwent hysterectomy due to benign diseases at Qilu Hospital (Table S5). Endometrial tissue from the entire uterine cavity was collected to establish endometrial organoids. Only proliferative endometrial tissue, confirmed by pathological diagnosis, was included in this study.

METHOD DETAILS

Human embryo thawing

Human blastocysts cryopreserved at day 5 post-fertilization(d.p.f. 5) were thawed using vitrification kits, following the manufacturer's instructions (VT602, KITAZATO BioPharma). Blastocysts were handled using a micropipetter and flexible tips. Open-pulled straws containing vitrified blastocysts were transferred directly from liquid nitrogen into 1 mL of pre-warmed thawing solution (TS). After 2 minutes in TS, blastocysts were released from the straw and transferred to the following solutions at room temperature: Dilution Solution (DS, 3 minutes for Kitazato), Washing Step 1 Solution (WS1, 5 minutes for Kitazato). After these steps, the embryos were placed in a droplet of embryo culture medium. The zona pellucida was mechanically dissected using a glass needle. The embryos were cultured in G-2 PLUS medium (10132, Vitrolife), covered with oil (10029, Vitrolife), and incubated at 37 °C with 5% O_2 and 6% CO_2 for at least 2 hours (ideally 5 hours) to embryo recovery.

Establishment of endometrial organoids

Endometrial tissue was collected using aseptic procedures and temporarily stored at 4 °C in pre-cooled collection medium (DMEM/F12 (Gibco, 11039021), 10% FBS (Sigma, F0926), and 1% antibiotics-antimycotics (Anti-Anti, Gibco, 15240-062)). The endometrium was washed with pre-chilled DPBS (Gibco, 14190136), blood clots were removed, and the tissue was minced in 1.5 mL EP tubes before adding digestion medium (0.4 mg/mL collagenase V (Sigma, C-9263), 1.25 U/mL dispase II (Sigma, D4693), and 10 μg/mL DNase I (Worthington, LS002139)). After digestion at 37 °C for 20 minutes, an equal volume of DMEM/F12 (with 10% FBS and 1% Anti-Anti) was added to neutralize the reaction. The suspension was left for 1 minute, then filtered through a 40 μm cell strainer (Corning, 352340). For cell collection, the strainer was inverted onto a culture dish and rinsed with DPBS. The resulting cell suspension was collected and centrifuged at 400 × *g* for 5 minutes. Cell pellets were washed twice with DMEM/F12 medium as described. An appropriate volume of DMEM/F12 was combined with the cell pellet, followed by the addition of Matrigel (Corning, 536231) using a pre-cooled pipette tip in a 1:3 ratio. The Matrigel-cell suspension was slowly seeded onto a preheated 24-well plate (Corning 3524) (40 μL/drop/well, 1 to 5 × 10^4 cells/drop) and incubated in a cell incubator at 37 °C for 30 minutes. Endometrial organoid growth medium (ExM) was then added to each well and changed every two days (Table S6).

Hormone treatment of endometrial organoids

Endometrial organoids were induced into the implantation window using ovarian steroid hormones, including estradiol (Sigma E2758), medroxyprogesterone acetate (MPA) (Selleck S2567), and N6, 2'-O-dibutyryladenosine 3', 5'-cyclic monophosphate sodium salt (cAMP) (Sigma D0627), as well as pregnancy-related hormones such as human chorionic gonadotropin (HCG) (Livzon Pharmaceutical Group Inc.), human placental lactogen (HPL) (R&D Systems 5757-PL), and prolactin (Peprotech 100-07). The specific

treatment protocol involved administering estradiol for two days, followed by a combination of estradiol, MPA, cAMP, HCG, HPL, and prolactin for a subsequent six-day period (Table S6).

Embryo-endometrium co-culture

Organoid droplets were carefully transferred intact into 4-well dishes (Corning, 354234) using a sterile pipette at room temperature. Each organoid droplet was fixed to the bottom of the dish with 5-10 μL of Matrigel (Corning, 354234), forming an organoid unit. The organoid unit was then placed in an incubator and allowed to incubate at 37 °C with 6% CO_2 and saturated humidity for 5 minutes, until the unit stabilized and ceased to shake. Following this, 500 μL of pre-balanced medium (HIVC1) (Table S7) was added to each well, and the dishes were returned to the incubator for one hour to facilitate implantation.

To accommodate a re-expanded d.p.f. 5 human blastocysts, the organoid droplet was lightly punctured with a needle to create a small pocket. Embryos were transferred into the organoid units using a sterile 150 μm glass pipette on a warm glass plate maintained at 37 °C, carefully adjusting the angle to ensure that the polar trophoblast rested against the side of the organoid. Embryos lacking a zona pellucida were cultured in 4-well dishes, with each well containing one embryo, one organoid unit, and 500 μL of pre-balanced medium (HIVC1). The co-culture units were incubated at 37 °C with 6% CO_2 and saturated humidity.

Embryos were cultured in a peri-implantation culture medium (Table S7). From d.p.f. 5.5 to 7, the culture medium used was HIVC1. At d.p.f. 8, 50% of the HIVC1 medium was replaced with HIVC2 medium. At d.p.f. 9, embryos were transferred to new wells containing HIVC2. Subsequently, 50% of the culture medium was replaced daily with fresh HIVC2 containing 10% Matrigel. HIVC1 and HIVC2 were pre-equilibrated in the incubator for a minimum of 6 hours prior to use.

Survival rate is defined as the percentage of embryos that meet both of the following conditions: (a) continued expansion in diameter from d.p.f. 5 to 14, and (b) no visible signs of apoptosis (such as cytoplasmic blebbing or membrane fragmentation), as observed through daily light microscopy.

Toluidine Staining

The samples were rinsed quickly with PBS buffer, and immediately fixed in 3% glutaraldehyde solution (pH 7.4). Following postfixation with 1% osmium tetroxide, dehydration and embedding with Epon812, the samples were sectioned for 1∼2 μm ultrathin sections using an ultramicrotome (LKB-V, LKB Company, Sweden). Sections were stained with toluene blue solution for 5 minutes, gently shaking to ensure uniform staining. Rinse the section gently with deionized water to remove excess dye, and observe the staining effect under a microscope.

Sample clearing, immunostaining and image analysis

The samples were washed in PBS and fixed in 4% paraformaldehyde (1710, Electron Microscopy Sciences) for 20 minutes at room temperature. After washing 3 times with PBS containing 0.1% (vol/vol) Tween-20 (PBST), the samples were incubated for 30 minutes with 0.3% (vol/vol) Triton X-100 (T8787 Sigma Aldrich) +0.1mM glycine (BP381-1, Thermo Fisher Scientific). Blocking buffer was used (PBST with 5% (w/vol) BSA, Sigma A9418), followed by overnight incubation at 4 °C with primary antibodies. The samples were then washed three times in PBST, incubated for two hours at room temperature with AlexaFluor secondary antibodies (1:500, Thermo Fisher Scientific) and DAPI (D3571, Thermo Fisher Scientific, 1 g/ml) diluted in blocking buffer.

To perform tissue clearing,[55] CUBIC-L, a reagent that degreases and decolorizes tissues, was used to clear the tissue. The fixed samples were then washed 3 times with PBS at room temperature. Samples were then soaked in pre-delipidation solution (a 1:1 mixture of ddH2O and CUBIC-L) and placed on a rotator at 37°C overnight. Afterward, the samples were washed three times in PBS at room temperature. They were then soaked overnight in ddH2O/CUBIC-L solution and placed on rotators at 37 °C. Following that, samples were placed in a 100% CUBIC-L solution on a rotator at 37 °C for 3-5 days. CUBIC-L was changed every day. The samples were then washed with PBS three times before immunostaining. The images were captured by the light-sheet microscope (Lightsheet7, Zeiss; LUXENDO, MuVi SPIM) and digital 3D reconstruction were performed via Imaris x64 10.0.1. The manual surface-rendering module was used for endometrium and embryo segmentation. The spots module was used for analysis of the nuclear localization signals.

Transmission electron microscopy (TEM) and Scanning electronic microscopy (SEM)

For transmission electron microscopy (TEM), the samples were rinsed quickly with PBS buffer, and immediately fixed in 3% glutaraldehyde solution (pH 7.4). Weiya Electron Microscopy Laboratory (Jinan, Shandong, China) performed the following experiments. Rinse sequentially according to standard TEM sample preparation procedures. Following postfixation with 1% osmium tetroxide, dehydration and embedding with Epon812, the samples were sectioned for 70∼100nm ultrathin sections using an ultramicrotome (LKB-V, LKB Company, Sweden). Sections were stained with lead citrate and uranyl acetate and observed under an electron microscope (JEM-1200EX; JEOL Ltd., Tokyo, Japan). Images were captured using a CCD camera (MORADA-G2, Olympus Corporation, Japan).

For scanning electron microscopy (SEM), cutted the tissue with a sharp blade, 1-3mm^3, identified and protected the observation surface, and fixed with 2.5% glutaraldehyde fixing solution for > 4 hours. The samples were soaked with 0.1ml phosphate buffer and fixed with 1% osmium tetroxide for 2 to 4 hours. The samples were soaked with double steaming water, dehydrated by ethanol gradient, vacuum dried by tert-butanol, and observed by Sigma300 thermal field emission scanning electron microscopy of ZESS.

Single-cell library preparation and sequencing

For smartseq2 sequencing,[56] the embryos were washed three times in PBS and twice in 0.25% trypsin (T4799, Sigma-Aldrich) before incubating with 0.25% trypsin for 15 minutes at 37°C and being terminated with FBS. By repeating pipetting, embryos were dissociated into individual cells and dispersed in 1% DFBS in PBS. One cell was manually selected and pipetted into a PCR tube. All operations were performed on a Nikon SMZ645 microscope.

For scRNA-seq, the embryos and organoids were washed three times in DPBS and were digested with GEXSCOPE@ Tissue Dissociation Solution(Singleron) at 37 °C for 15 minutes with sustained agitation. The cell suspension was centrifuged at 350 × *g* for 5 min, the supernatant was discarded, and the cell precipitate was resuspended with 1mL of PBS (Basal Media), and washed again by adding PBS to fix the volume, and then centrifuged at 300 × *g* for 5 min, the supernatant was discarded, and the cell precipitate was resuspended with an appropriate amount of PBS. The sample was stained with trypan blue (Sigma, Shanghai, China) and microscopically evaluated for cell viability. Single-cell suspensions with 1×10^5 cells/ml in PBS (HyClone, Shanghai, China) were prepared and loaded onto microfluidic devices. Then scRNA-seq libraries were constructed according to Singleron GEXSCOPE® protocol by GEXSCOPE® Single-Cell RNA Library Kit (Singleron Biotechnologies) and Singleron Matrix® Automated single-cell processing system (Singleron Biotechnologies). Individual libraries were diluted to 4ng/μL and pooled for sequencing. Pools were sequenced on Illumina novaseq6000 with 150 bp paired end reads.

Quality control, dimension-reduction and clustering

Scanpy v1.8.1[54]was used for quality control, dimensionality reduction and clustering under Python 3.7. For each sample dataset, we filtered expression matrix by the following criteria: 1) cells with gene count less than 200 or with top 2% gene count were excluded; 2) cells with top 2% UMI count were excluded; 3) cells with mitochondrial content>20% were excluded; 4) genes expressed in less than 5 cells were excluded. After filtering, E-EO cells were retained for the downstream analyses. The raw count matrix was normalized by total counts per cell and logarithmically transformed into normalized data matrix. Top 2000 variable genes were selected by setting flavor = 'seurat'. Principle Component Analysis (PCA) was performed on the scaled variable gene matrix, and top 20 principle components were used for clustering and dimensional reduction. Cells were separated into different clusters by using Louvain algorithm and setting resolution parameter. Cell clusters were visualized by using Uniform Manifold Approximation and Projection (UMAP).

Differentially expressed genes (DEGs) analysis

To identify differentially expressed genes (DEGs), we used the scanpy.tl.rank_genes_groups function based on Wilcoxon rank-sum test with default parameters, and selected the genes expressed in more than 10% of the cells in either of the compared groups of cells and with an average log(Fold Change) value greater than 0.25 as DEGs. Adjusted p value was calculated by Benjamini-Hochberg correction and the value 0.05 was used as the criterion to evaluate the statistical significance.

Cell-cell communication analysis

To compare the changes of the cell-cell interactions among TE, and EO between the co-culture and separate culture conditions, we performed cell-cell communication analysis using the Cellphone DB v4 package.[45] Permutation number for calculating the null distribution of average ligand-receptor pair expression in randomized cell identities was set to 1000. Individual ligand or receptor expression was thresholded by a cutoff based on the average log gene expression distribution for all genes across each cell type. Predicted interaction pairs with p value <0.05 and of average log expression > 0.1 were considered as significant and visualized by heatmap_plot and dot_plot in CellphoneDB.

Pseudotime construction

Monocle2 Cell differentiation trajectory was reconstructed with the Monocle2 (v 2.22.).[57] For constructing the trajectory, top 2000 highly variable genes were selected by Seurat[58] (v4.1.0), FindVairableFeatures, and dimension-reduction was performed by DDRTree. The trajectory was visualized by plot_cell_trajectory function in Monocle2. For the EVTs subpopulation, pseudotime trajectory analysis was performed using the Diffusion Pseudotime (DPT)[59] algorithm implemented in Scanpy (v1.9.1). Specifically, the scanpy.tl.dpt function was used to infer pseudotime along a diffusion map-based manifold. A putative EVT1 cell was designated as the root cell to initialize the trajectory, as specified by adata.uns[''iroot'']. The resulting pseudotime values were visualized using UMAP embedding via the scanpy.pl.umap function, with cells colored according to their progression along the inferred trajectory.

Comparison analysis with published available datasets

The expression matrices of published datasets and our dataset were combined (10x single-cell data of d.p.f 8-10-12-14 embryos,[52] 10x scRNA-seq data from d.p.f 9–11 embryos,[53] smartseq2 data from d.p.f 14 embryos.[4] Cells and genes were filtered with the same standards as described in the PHATE embedding section. The median-normalized matrix was natural-log-transformed with the addition of a pseudocount of 1. The resulting matrix was zero-centred and scaled per gene (standard deviation is 1) before PCA.

Batch correction

The Harmony algorithm was used to integrate human post-implantation embryo datasets with our datasets, using default parameters (Python implementation v.1.0.0; https://github.com/slowkow/harmonypy). Sample information was used for correction. The CellHint[60]

algorithm was used to integrate human trophoblast datasets with our datasets, using default parameters (Python implementation v.1.0.0; https://github.com/Teichlab/cellhint). Integration was performed using the 'gname' annotation as batch information and 'cluster' as biological reference, with the number of meta-neighbors set to 1 (n_meta_neighbors=1). Batch processing is not only in the integration of public data and free data, but also in the integration of free data. After parameter viewing, the batch processing here is a batch processing based on the sample information. Following integration, dimensionality reduction was performed using UMAP (Scanpy v.1.10.1), computed on the corrected neighborhood graph with default parameters.

Spatial proteomics

Sample was obtained from a d.p.f. 9 co-cultured embryo and then washed with PBS. After excess PBS on the WE sample, the sample was soaked in liquid nitrogen pre-cooled isopentane for 1 min and then was transferred in O.C.T. Compound (Solarbio, China) and snap frozen. The O.C.T.-embedded tissue was sectioned at 10 μm on a CM1950 cryostat (Leica) and mounted onto PEN membrane-coated glass slides. The tissue sections were stained with hematoxylin and eosin (H&E). Laser-capture microdissection procedure was completed on Laser-Capture Microdissection System PALM (Zeiss). The regions of interest (ROI) containing a specific cell type in the section was marked with LCM marker pen and microdissected using above mentioned settings and collected with microtubes (Zeiss, 415190-9201-000). The three ROI selected for analysis in this study include the solo embryo part, the endometrium organoid part, and the maternal-fetal contact part. The microdissected samples were digested for proteomic. Consequently, the samples were processed for microproteomics and analyzed using mass spectrometry according to the service provider's guidelines (PTM Biolabs ins). The resulting MS/MS data were processed using MaxQuant search engine (v.1.6.15.0). Tandem mass spectra were searched against the human SwissProt database (20422 entries) concatenated with reverse decoy database. FDR was adjusted to $< 1\%$. We used the functions enrichKEGG and enrichGO in clusterProfiler R package[61] to perform KEGG pathways and Gene Ontology (GO) biological processes enrichment analysis. A pathway or process with a p value ≤ 0.05 was considered to be significantly enriched. The enriched pathways and processes were visualized with the ''ggplot'' function in the ggplot2 package in R. All differentially expressed protein database accession or sequence were searched against the STRING database version 11.5 for protein-protein interactions. Only interactions between the proteins belonging to the searched data set were selected, thereby excluding external candidates. STRING defines a metric called ''confidence score'' to define interaction confidence; we fetched all interactions that had a confidence score ≥ 0.7 (high confidence).